2.3 STM and SFM

Scanning Tunneling Microscopy and Scanning Force Microscopy

REBECCA S. HOWLAND AND MICHAEL D. KIRK

Contents

Introduction

Scanning Tunneling Microscopy (STM) and its offspring, Scanning Force Microscopy (SFM), are real-space imaging techniques that can produce topographic images of a surface with atomic resolution in all three dimensions. Almost any solid surface can be studied with STM or SFM: insulators, semiconductors, and conductors, transparent as well as opaque materials. Surfaces can be studied in air, in liquid, or in ultrahigh vacuum, with fields of view from atoms to greater than 250 × 250 μm. With this flexibility in both the operating environment and types of samples that can be studied, STM / SFM is a powerful imaging system.

The scanning tunneling microscope was invented at IBM, Zurich, by Gerd Binnig and Heinrich Rohrer in 1981.[1] In ultrahigh vacuum, they were able to resolve the atomic positions of atoms on the surface of Si (111) that had undergone a 7 × 7 reconstruction (Figure 1). With this historic image they solved the puzzle of the atomic structure of this well studied surface, thereby establishing firmly the credibility and importance of this form of microscopy. For the invention of STM, Binnig and Rohrer earned the Nobel Prize for Physics in 1986.

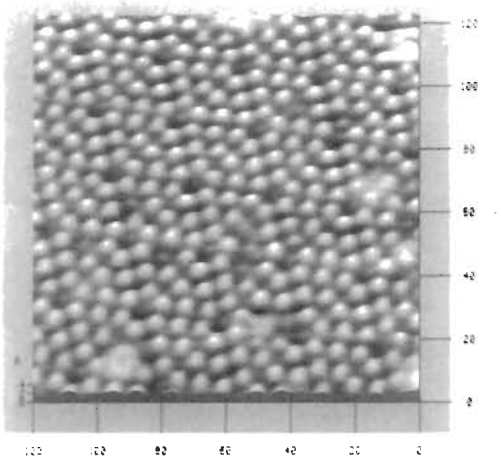

Figure 1 **Ultrahigh-vacuum STM image of Si (111) showing 7 × 7 reconstruction.**

Since then, STM has been established as an instrument for forefront research in surface physics. Atomic resolution work in ultrahigh vacuum includes studies of metals, semimetals and semiconductors. In particular, ultrahigh-vacuum STM has been used to elucidate the reconstructions that Si, as well as other semiconducting and metallic surfaces undergo when a submonolayer to a few monolayers of metals are adsorbed on the otherwise pristine surface.[2]

Because STM measures a quantum-mechanical tunneling current, the tip must be within a few Å of a conducting surface. Therefore any surface oxide or other contaminant will complicate operation under ambient conditions. Nevertheless, a great deal of work has been done in air, liquid, or at low temperatures on inert surfaces. Studies of adsorbed molecules on these surfaces (for example, liquid crystals on highly oriented, pyrolytic graphite[3]) have shown that STM is capable of even atomic resolution on organic materials.

The inability of STM to study insulators was addressed in 1985 when Binnig, Christoph Gerber and Calvin Quate invented a related instrument, the scanning force microscope.[4] Operation of SFM does not require a conducting surface; thus insulators can be studied without applying a destructive coating. Furthermore, studying surfaces in air is feasible, greatly simplifying sample preparation while reducing the cost and complexity of the microscope.

STM and SFM belong to an expanding family of instruments commonly termed Scanning Probe Microscopes (SPMs). Other common members include the magnetic force microscope, the scanning capacitance microscope, and the scanning acoustic microscope.[5]

Although the first six or seven years of scanning probe microscope history involved mostly atomic imaging, SPMs have evolved into tools complementary to Scanning and Transmission Electron Microscopes (SEMs and TEMs), and optical and stylus profilometers. The change was brought about chiefly by the introduction of the ambient SFM and by improvements in the range of the piezoelectric scanners that move the tip across the sample. With lateral scan ranges on the order of 250 μm, and vertical ranges of about 15 μm, STM and SFM can be used to address larger scale problems in surface science and engineering in addition to atomic-scale research. STM and SFM are commercially available, with several hundred units in place worldwide.

SPMs are simpler to operate than electron microscopes. Because the instruments can operate under ambient conditions, the set-up time can be a matter of minutes. Sample preparation is minimal. SFM does not require a conducting path, so samples can be mounted with double-stick tape. STM can use a sample holder with conducting clips, similar to that used for SEM. An image can be acquired in less than a minute; in fact, "movies" of ten frames per second have been demonstrated.[6]

The three-dimensional, quantitative nature of STM and SFM data permit in-depth statistical analysis of the surface that can include contributions from features 10 nm across or smaller. By contrast, optical and stylus profilometers average over areas a few hundred Å across at best, and more typically a μm. Vertical resolution for SFM/STM is sub-Å, better than that of other profilometers. STM and SFM are excellent high-resolution profilometers.

STM and SFM are free from many of the artifacts that afflict other kinds of profilometers. Optical profilometers can experience complicated phase shifts when materials with different optical properties are encountered. The SFM is sensitive to topography only, independent of the optical properties of the surface. (STM may be sensitive to the optical properties of the material inasmuch as optical properties are related to electronic structure.) The tips of traditional stylus profilometers exert forces that can damage the surfaces of soft materials, whereas the force on SFM tips is many orders of magnitude lower. SFM can image even the tracks left by other stylus profilometers.

In summary, scanning probe microscopes are research tools of increasing importance for atomic-imaging applications in surface science. In addition, SFM and STM are now used in many applications as complementary techniques to SEM, TEM, and optical and stylus profilometry. They meet or exceed the performance of these instruments under most conditions, and have the advantage of operating in an ambient environment with little or no sample preparation. The utility of scanning probe microscopy to the magnetic disk, semiconductor, and the polymer industries is gaining recognition rapidly. Further industrial applications include the analysis of optical components, mechanical parts, biological samples, and other areas where quality control of surfaces is important.

STM

Scanning tunneling microscopes use an atomically sharp tip, usually made of tungsten or Pt-Ir. When the tip is within a few Å of the sample's surface, and a bias voltage V_t is applied between the sample and the tip, quantum-mechanical tunneling takes place across the gap. This tunneling current I_t depends exponentially on the separation d between the tip and the sample, and linearly on the local density of states. The exponential dependence of the magnitude of I_t upon d means that, in most cases, a single atom on the tip will image the single nearest atom on the sample surface.

The quality of STM images depends critically on the mechanical and electronic structure of the tip. Tungsten tips are sharpened by electrochemical etching, and can be used for a few hours in air, until they oxidize. On the other hand, Pt-Ir tips can be made by stretching a wire and cutting it on an angle with wire cutters. These tips are easy to make and slow to oxidize, but the resulting tip does not have as high an aspect ratio as a tungsten tip. As a result, Pt-Ir tips are not as useful for imaging large structures.

In its most common mode of operation, STM employs a piezoelectric transducer to scan the tip across the sample (Figure 2a). A feedback loop operates on the scanner to maintain a constant separation between the tip and the sample. Monitoring the position of the scanner provides a precise measurement of the tip's position in three dimensions. The precision of the piezoelectric scanning elements, together with the exponential dependence of I_t upon d means that STM is able to provide images of individual atoms.

Because the tunneling current also depends on the local density of states, STM can be used for spatially resolved spectroscopic measurements. When the component atomic species are known, STM can differentiate among them by recording and comparing multiple images taken at different bias voltages. One can ramp the bias voltage between the tip and the sample and record the corresponding change in the tunneling current to measure I versus V or dI/dV versus V at specific sites on the image to learn directly about the electronic properties of the surface. Such measurements give direct information on the local density of electronic states. This technique was pioneered by Hamers, et al., who used tunneling spectroscopy to map the local variations in the bonding structure between Si atoms on a reconstructed surface.[7]

On the other hand, the sensitivity of STM to electronic structure can lead to undesired artifacts when the surface is composed of regions of varying conductivity. For example, an area of lower conductivity will be represented as a dip in the image. If the surface is not well known, separating topographic effects from electronic effects can be difficult.

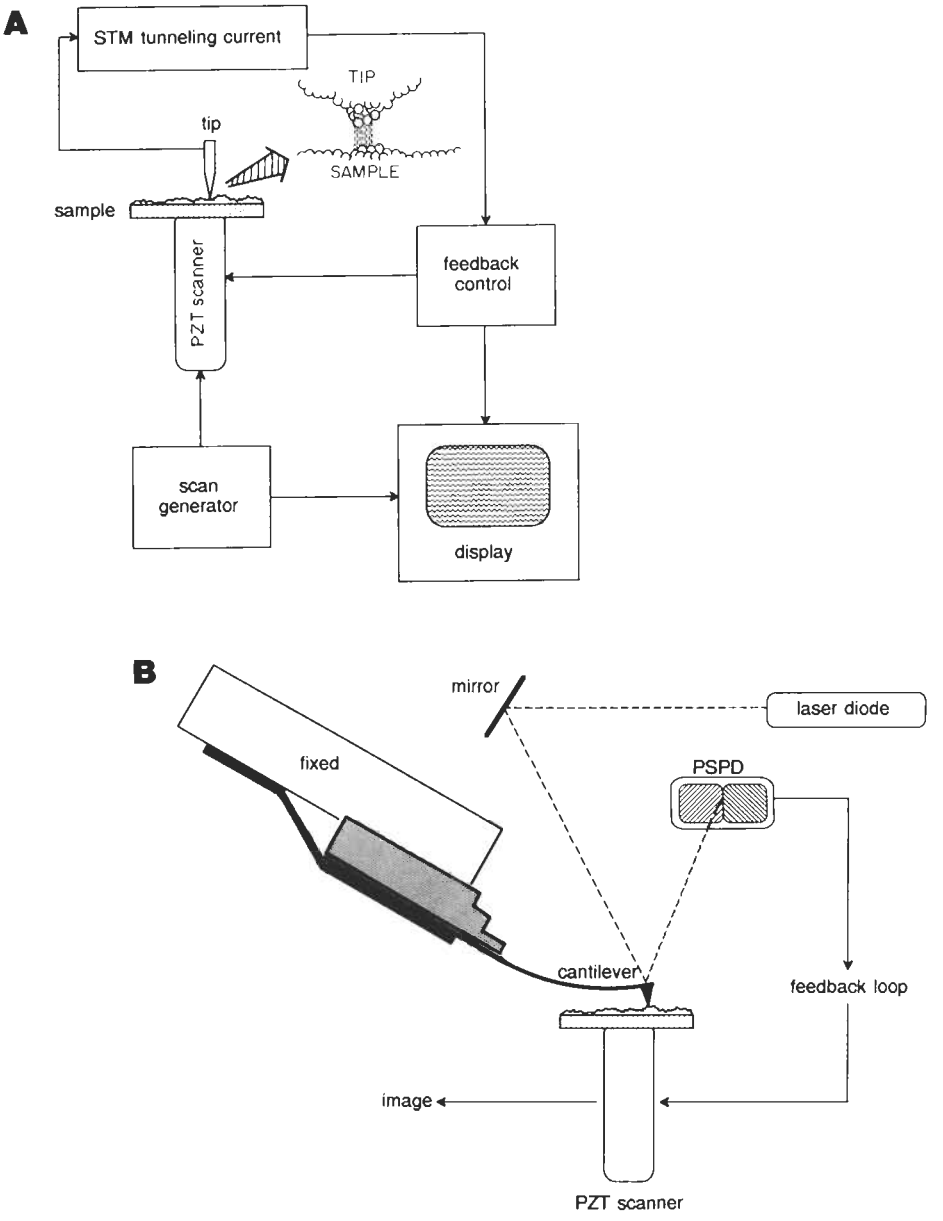

Figure 2 **Schematic of STM (a) and SFM (b).**

SFM

Scanning force microscopes use a sharp tip mounted on a flexible cantilever. When the tip comes within a few Å of the sample's surface, repulsive van der Waals forces

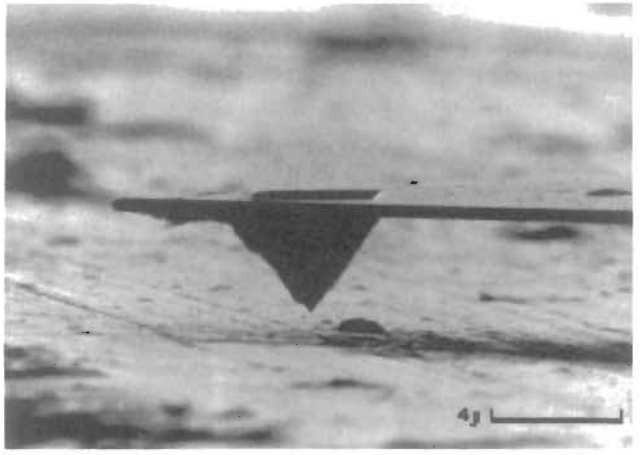

Figure 3 **SEM image of SFM cantilever showing pyramidal tip.**

between the atoms on the tip and those on the sample cause the cantilever to deflect. The magnitude of the deflection depends on the tip-to-sample distance *d*. However, this dependence is a power law, that is not as strong as the exponential dependence of the tunneling current upon *d* employed by STM. Thus several atoms on an SFM tip will interact with several atoms on the surface. Only with an unusually sharp tip and flat sample is the lateral resolution truly atomic; normally the lateral resolution of SFM is about 1nm.

Like STM, SFM employs a piezoelectric transducer to scan the tip across the sample (Figure 2b), and a feedback loop operates on the scanner to maintain a constant separation between the tip and the sample. As with STM, the image is generated by monitoring the position of the scanner in three dimensions.

For SFM, maintaining a constant separation between the tip and the sample means that the deflection of the cantilever must be measured accurately. The first SFM used an STM tip to tunnel to the back of the cantilever to measure its vertical deflection. However, this technique was sensitive to contaminants on the cantilever.[4] Optical methods proved more reliable. The most common method for monitoring the defection is with an optical-lever or beam-bounce detection system.[8] In this scheme, light from a laser diode is reflected from the back of the cantilever into a position-sensitive photodiode. A given cantilever deflection will then correspond to a specific position of the laser beam on the position-sensitive photodiode. Because the position-sensitive photodiode is very sensitive (about 0.1 Å), the vertical resolution of SFM is sub-Å.

Figure 3 shows an SEM micrograph of a typical SFM cantilever. The cantilevers are 100–200 μm long and 0.6 μm thick, microfabricated from low-stress Si_3N_4 with an integrated, pyramidal tip. Despite a minimal tip radius of about 400 Å,

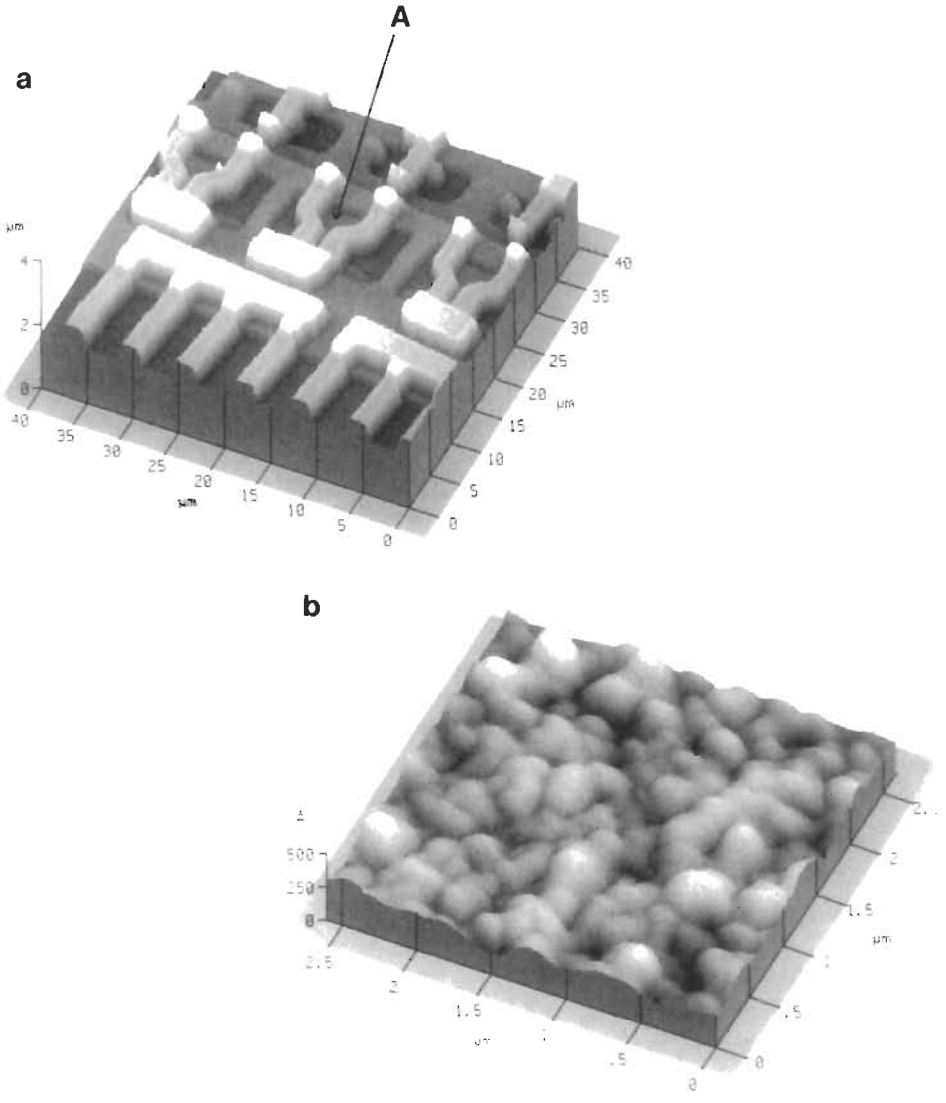

Figure 4 **SFM image of an integrated circuit (a) and close-up of silicon oxide on its surface (b).**

which is needed to achieve high lateral resolution, the pressure exerted on the sample surface is small because of the low force constant of the cantilever (typically 0.2 N / m), and the high sensitivity of the position-sensitive photodiode to cantilever deflection. The back of the cantilever may be coated with gold or another metal to enhance the reflectance of the laser beam into the detector.

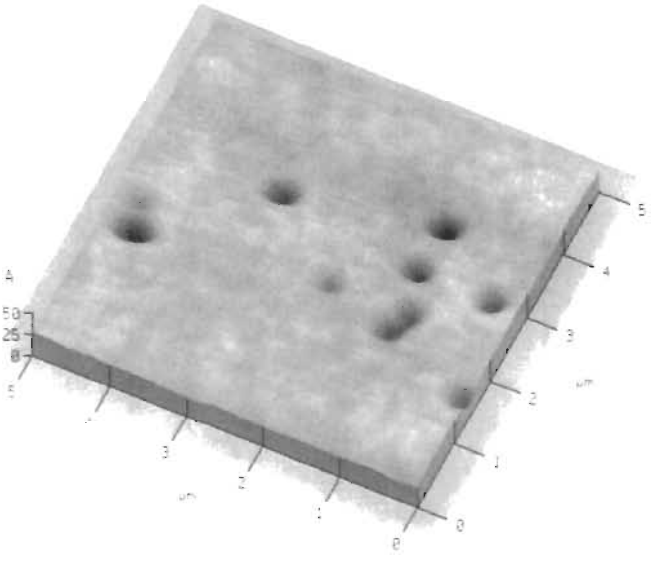

Figure 5 **SFM image of oxidized Si wafer showing pinhole defects 20 Å deep.**

Common Modes of Analysis and Examples

STM and SFM are most commonly used for topographic imaging, three-dimensional profilometry and spectroscopy (STM only).

Topography

Unlike optical or electron microscopes, which rely on shadowing to produce contrast that is related to height, STM and SFM provide topographic information that is truly three-dimensional. The data are digitally stored, allowing the computer to manipulate and display the data as a three-dimensional rendition, viewed from any altitude and azimuth. For example, Figure 4a shows an SFM image of an integrated circuit; Figure 4b is a close-up of the oxide on the surface of the chip in the region marked *A* in Figure 4a. In a similar application, Figure 5 is an SFM image of a Si wafer with pinholes, 20 Å deep. Easily imaged with SFM, these pinholes cannot be detected with SEM.

Profilometry

The three-dimensional, digital nature of SFM and STM data makes the instruments excellent high-resolution profilometers. Like traditional stylus or optical profilometers, scanning probe microscopes provide reliable height information. However, traditional profilometers scan in one dimension only and cannot match SPM's height and lateral resolution.

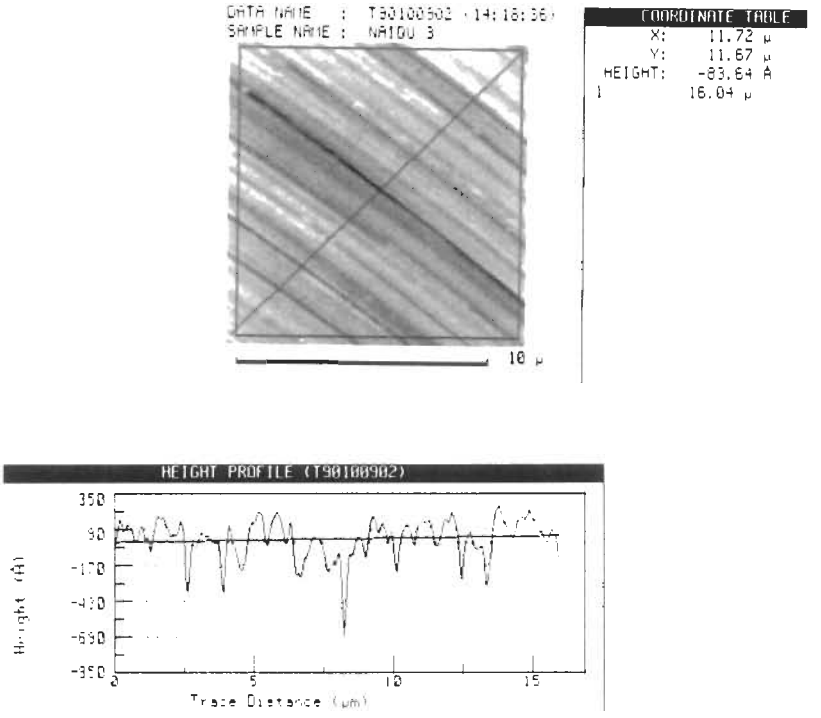

Figure 6 **SFM image of a magnetic storage disk demonstrating roughness analysis.**

In the magnetic storage disk industry, the technology has advanced to the point where surface roughness differences on the order of a few Å have become important. Optical and stylus profilometers, while still preferable for scanning very large distances, cannot measure contributions from small features. Figure 6 is an SFM image of a thin-film storage disk (top), shown top-down, with heights displayed in a linear intensity scale ("gray scale"). Using the mouse, the height profile of any cross section can be displayed and analyzed (bottom). Figure 7 shows a thin-film read–write head. The magnetic poles are recessed about 200 Å; their roughness is comparable to that of the surrounding medium. Note the textural difference between the glass embedding medium and the ceramic. SFM is not affected by differences in optical properties when it scans composite materials.

Profilometry of softer materials, such as polymers, is also possible with SFM, and with STM if the sample is conducting. Low forces on the SFM tip allow imaging of materials whose surfaces are degraded by traditional stylus profilometry. However, when the surface is soft enough that it deforms under pressure from the SFM tip, resolution will be degraded and topography may not be representative of the true

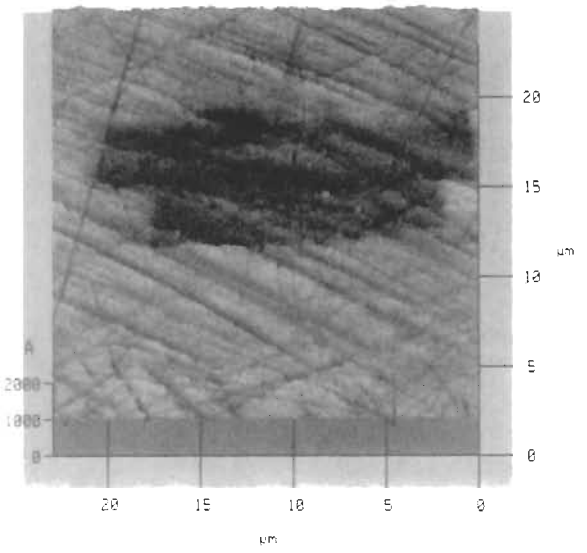

Figure 7 **SFM image of a thin-film read–write head showing magnetic poles (dark rectangles) recessed 200 Å.**

surface. One can investigate the reproducibility of the image by scanning the sample in different directions at various scan rates and image sizes.

Spectroscopy

The preceding topography and profilometry examples have focused on the scanning force microscope. STM also can be used for topographic imaging and profilometry, but the images will be convolutions of the topographic and electronic structure of the surface. A similar effect is seen with SEM, arising from differences in secondary electron coefficients among different materials.

Taking advantage of the sensitivity of the tunneling current to local electronic structure, the STM can be used to measure the spectra of surface-state densities directly. This can be accomplished by measuring the tunneling current as a function of the bias voltage between the tip and sample, or the conductivity, dI/dV, versus the bias voltage, at specific spatial locati ɔns on the surface. Figure 8 is a spectroscopic study of GaAs(110). The image on the left was taken with negative bias voltage on the STM tip, which allows tunneling into unoccupied states, thereby revealing the Ga atoms. Taken simultaneously but with a positive tip bias voltage, the image on the right results from tunneling out occupied states, and shows the positions of the As atoms.

The data above were collected in UHV environment to achieve the most pristine surface. Spectroscopy in air is usually more difficult to interpret due to contamination with oxides and other species, as is the case with all surface-sensitive spectroscopies.

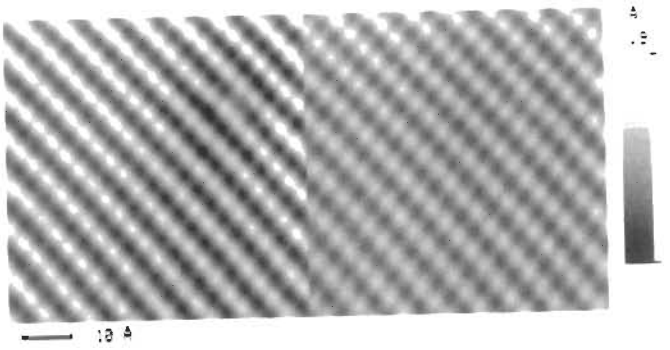

Figure 8 **Spectroscopic study of GaAs(110). With a positive voltage on the STM tip, the left-hand image represents As atoms, while the corresponding negative tip voltage on the right shows Ga atoms. (Courtesy of Y. Yang and J.H. Weaver, University of Minnesota)**

Sample Requirements

For atomic resolution an atomically flat sample is required to avoid tip imaging (see below). STM requires a conducting surface to establish the tunneling current. Doped Si has sufficient conductivity to enable STM imaging, but surfaces of lower conductivity may require a conductive coating. SFM can image surfaces of any conductivity. Both STM and SFM require solid surfaces that are somewhat rigid; otherwise the probes will deform the surfaces while scanning. Such deformation is easily diagnosed by repeatedly scanning the same area and noting changes.

The deformation of soft surfaces can be minimized with SFM by selecting cantilevers having a low force constant or by operating in an aqueous environment. The latter eliminates the viscous force that arises from the thin film of water that coats most surfaces in ambient environments. This viscous force is a large contributor to the total force on the tip. Its elimination means that the operating force in liquid can be reduced to the order of 10^{-9} N.

An example, Figure 9 is an SFM image of a Langmuir-Blodgett film. This film was polymerized with ultraviolet light, giving a periodicity of 200 Å, which is seen in the associated Fourier transform. The low forces exerted by the SFM tip are essential for imaging such soft polymer surfaces.

Poorly cleaned surfaces may not image well. While ordinary dry dust will be brushed aside by the tip and will not affect the image, oily or partially anchored dirt will deflect the SFM tip or interfere with the conductivity in STM. The result is usually a line smeared in the scan direction, exactly as one would expect if the tip began scanning something which moved as it was scanned. If the sample cannot be cleaned, the best procedure is to search for a clean area.

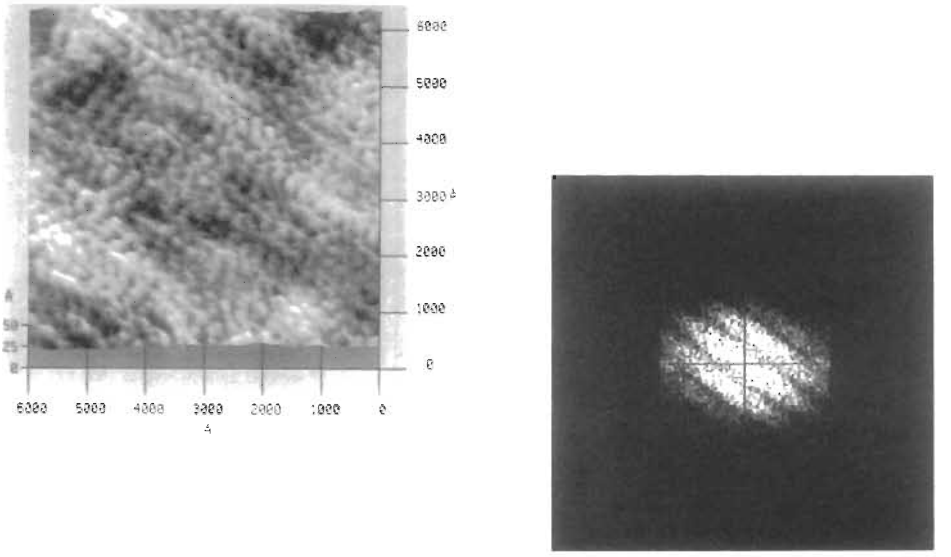

Figure 9 **SFM image of Langmuir-Blodgett film (top) and associated Fourier transform (bottom). (Courtesy of T. Kato, Utsunomiya University)**

Maximum sample sizes that can be accommodated by SFM or STM vary. Current systems can scan a 8-inch Si wafer without cutting it. When industry calls for the capability to scan larger samples, the SPM manufacturers are likely to respond.

Artifacts

The main body of artifacts in STM and SFM arises from a phenomenon known as *tip imaging*.[9] Every data point in a scan represents a convolution of the shape of the tip and the shape of the feature imaged, but as long as the tip is much sharper than the feature, the true edge profile of the feature is represented. However, when the feature is sharper than the tip, the image will be dominated by the edges of the tip. Fortunately, this kind of artifact is usually easy to identify.

Other artifacts that have been mentioned arise from the sensitivity of STM to local electronic structure, and the sensitivity of SFM to the rigidity of the sample's surface. Regions of variable conductivity will be convolved with topographic features in STM, and soft surfaces can deform under the pressure of the SFM tip. The latter can be addressed by operating SFM in the attractive mode, at some sacrifice in the lateral resolution. A limitation of both techniques is their inability to distinguish among atomic species, except in a limited number of circumstances with STM microscopy.

STM

In STM, the tip is formed by an atom or cluster of atoms at the end of a long wire. Because the dependence of the tunneling current upon the tip-to-sample distance is exponential, the closest atom on the tip will image the closest atom on the sample. If two atoms are equidistant from the surface, all of the features in the image will appear doubled. This is an example of multiple tip imaging. The best way to alleviate this problem is to collide the tip gently with the sample, to form a new tip and take another image. Alternatively, a voltage pulse can be applied to change the tip configuration by field emission.

STM tips will last for a day or so in ultrahigh vacuum. Most ultrahigh-vacuum STM systems provide storage for several tips so the chamber does not have to be vented just to change tips. In air, tips will oxidize more rapidly, but changing tips is a simple process.

SFM

At present, all commercial SFM tips are square pyramids, formed by CVD deposition of Si_3N_4 on an etch pit in (100) Si. The etch pit is bounded by (111) faces, which means that the resulting tip has an included angle of about 55°. Therefore the edge profiles of all features with sides steeper than 55° will be dominated by the profile of the tip.

Because many kinds of features have steep sides, tip imaging is a common plague of SFM images. One consolation is that the height of the feature will be reproduced accurately as long as the tip touches bottom between features. Thus the roughness statistics remain fairly accurate. The lateral dimensions, on the other hand, can provide the user with only an upper bound.

Another class of artifacts occurs when scanning vertical or undercut features. As the tip approaches a vertical surface, the side wall may encounter the feature before the end of the tip does. The resulting image will appear to contain a discontinuous shift. Changing the angle of the tip with respect to the sample's surface can minimize the problem. Side wall imaging also occurs in STM, but less frequently since an STM tip has a higher aspect ratio than that of an SFM tip.

Improving the aspect ratio of SFM tips is an area of active research. A major difficulty is that the durability of the tip likely will be compromised as aspect ratios are increased.

Conclusions

Scanning probe microscopy is a forefront technology that is well established for research in surface physics. STM and SFM are now emerging from university laboratories and gaining acceptance in several industrial markets. For topographic analysis and profilometry, the resolution and three-dimensional nature of the data is

unequalled by other techniques. The ease of use and nondestructive nature of the imaging are notable.

The main difficulty with STM and SFM techniques is the problem of tip imaging. Neither technique is recommended for obtaining accurate measurements of edge profiles of vertical or undercut surfaces. In addition, SFM tips cannot accurately image the lateral dimensions of features with sides steeper than 55° at present. Obtaining SFM tips with more suitable aspect ratios is an area of active research.

Scanning tunneling and scanning force microscopes are only two members of the family of scanning probe microscopes. Other types of scanning probe microscopes may become widely used in the near future. The magnetic force microscope, for example, may one day be used routinely to study magnetic domains in storage media.

Related Articles in the Encyclopedia

Light Microscopy, SEM, TEM, STEM, and Surface Roughness

References

1 G. Binnig, H. Rohrer, C. Gerber, and E. Weibel. *Phys. Rev. Lett.* **49,** 57, 1982.

2 D. Rugar and P. Hansma. *Physics Today*. October, 23, 1990.

3 J. S. Foster and J. E. Frommer. *Nature.* **333,** 542, 1988.

4 G. Binnig, C. F. Quate, and C. Gerber. *Phys. Rev. Lett.* **54,** 930, 1986.

5 H. K. Wickramsinghe. *Scientific American*. October, 98, 1989.

6 R. Barret and C. F. Quate. To be published.

7 R. J. Hamers, R. M. Tromp, and J. E. Demuth. *Phys. Rev. Lett.* **56,** 1972, 1986.

8 G. Meyer and N. M. Amer. *Appl. Phys. Lett.* **53,** 1045, 1988.

9 S.-I. Park, J. Nogami, and C. F. Quate. *Phys. Rev. B* **36,** 2863, 1987.

5

ELECTRON EMISSION SPECTROSCOPIES

5.0 INTRODUCTION

In this chapter we have collected together those techniques in which one measures the energy distribution of electrons ejected from a material. In all four techniques covered electronic energy level excitations are involved, providing atomic or chemical state identification, or both. All are also true surface techniques, since the energies of the electrons concerned fall in the range where they travel can only very short distances without being inelastically scattered. These techniques are all sensitive to less than monolayer amounts of material and none have probing depths greater than about 50 Å without using sputter profiling.

The first two techniques discussed, X-Ray Photoelectron Spectroscopy, XPS, (also known as Electron Spectroscopy for Chemical Analysis, ESCA) and Ultraviolet Photoelectron Spectroscopy, UPS, are very closely related. XPS involves soft X rays (usually 1486 eV, from an Al anode) ejecting photoelectrons from the sample. Electrons originating from the core levels identify the elements present from their Binding Energies, BE. Small "chemical shifts" in the BEs provide additional chemical state information. The relative concentrations of the different elements present can be determined from relative peak intensities. XPS identifies all elements except hydrogen and helium from a depth ranging from around 2 monolayers to 25 monolayers. Typical values for XPS peaks in the 500–1400 eV kinetic energy range are 5 to 10 monolayers.

The strengths of XPS are its good quantification, its excellent chemical state determination capabilities, its applicability to a wide variety of materials from biological materials to metals, and its generally nondestructive nature. XPS's weaknesses are its lack of good spatial resolution (70 μm), only moderate absolute sensitivity (typically 0.1 at. %), and its inability to detect hydrogen. Commercial XPS instruments are usually fully UHV compatible and equipped with accessories, including a sputter profile gun. Costs vary from $250,000 to $600,000, or higher if other major techniques are included.

UPS differs from XPS only in that it uses lower energy radiation to eject photoelectrons, typically the 21.2-eV and 40.8-eV radiation from a He discharge lamp, or up to 200 eV at synchrotron facilities. The usual way to perform UPS is to add a He lamp to an existing XPS system, at about an incremental cost of $30,000. Most activity using UPS is in the detailed study of valence levels for electronic structure information. For materials analysis it is primarily useful as an adjunct to XPS to look at the low-lying core levels that can be accessed by the lower energy UPS radiation sources. There are several advantages in doing this: a greater surface sensitivity because the electron kinetic energies are lower, better energy resolution because the source has a narrower line width, and the possibility of improved lateral resolution using synchrotron sources.

Auger Electron Spectroscopy, AES, is also closely related to XPS. The hole left in a core level after the XPS process, is filled by an electron dropping from a less tightly bound level. The energy released can be used to eject another electron, the Auger electron, whose energy depends only on the energy levels involved and not on whatever made the initial core hole. This allows electrons, rather than X rays, to be used to create the initial core hole, unlike XPS. Since all the energy levels involved are either core or valence levels, however, the type of information supplied, like XPS, is elemental identification from peak positions and chemical state information from chemical shifts and line shapes. The depths probed are also similar to XPS. Dedicated AES systems for materials analysis, which are of similar cost to XPS instruments, have electron optics columns producing finely focused, scannable electron beams of up to 30 kV energy and beam spot sizes as small as 200 Å, a great advantage over XPS. AES could have been discussed in Chapter 3 along with STEM, EMPA, etc. When the incident beam is scanned over the sample (Scanning Auger Microprobe, SAM) mapping at high spatial resolution is obtained. For various reasons the area analyzed is always larger than the spot size, the practical limit to SAM being in the 300–1000 Å range. Another advantage of AES over XPS is speed, since higher electron beam currents can be used. There are major disadvantages to using electrons, however. Beam damage is often severe, particularly for organics, where desorption or decomposition often occurs under the beam. Sample charging for insulators is also a problem. Overall, the two techniques are about equally widespread and are the dominant methods for nontrace level analysis at surfaces. AES is the choice for inorganic systems where high spatial resolution is needed (e.g., semi-

conductor devices) and XPS should be one's choice otherwise. Combined systems are quite common.

Reflected Electron Energy-Loss Spectroscopy, REELS, is a specialized adjunct to AES, just as UPS is to XPS. A small fraction of the primary incident beam in AES is reflected from the sample surface after suffering discrete energy losses by exciting core or valence electrons in the sample. This fraction comprises the electron energy-loss electrons, and the values of the losses provide elemental and chemical state information (the Core Electron Energy-Loss Spectra, CEELS) and valence band information (the Valence Electron Energy-Loss Spectra, VEELS). The process is identical to the transmission EELS discussed in Chapter 3, except that here it is used in reflection, (hence REELS, reflection EELS), and it is most useful at very low beam energy (e.g., 100 eV) where the probing depth is at a very short minimum (as in UPS). Using the rather high-intensity VEELS signals, a spatial resolution of a few microns can be obtained in mapping mode at 100-eV beam energy. This can be improved to 100 nm at 2-keV beam energy, but the probing depth is now the same as for XPS and AES. Like UPS, VEELS suffers in that there is no direct elemental analysis using valence region transitions, and that peaks are often overlapped. The technique is free on any AES instrument and has been used to map metal hydride phases in metals and oxides at grain boundaries at the 100-nm spatial resolution level.

5.1 XPS

X-Ray Photoelectron Spectroscopy

C. R. BRUNDLE

Contents

Introduction

The photoelectric process, discovered in the early 1900s, was developed for analytical use in the 1960s, largely due to the pioneering work of Kai Siegbahn's group.[1] Important steps were the development of better electron spectrometers, the realization that electron binding energies were sensitive to the chemical state of the atom, and that the technique was surface sensitive. This surface sensitivity, combined with quantitative and chemical state analysis capabilities have made XPS the most broadly applicable general surface analysis technique today. It can detect all elements except hydrogen and helium with a sensitivity variation across the periodic table of only about 30. Samples can be gaseous, liquid, or solid, but the vast majority of electron spectrometers are designed to deal with solids. The depth of the solid material sampled varies from the top 2 atomic layers to 15–20 layers. The area examined can be as large as 1 cm × 1 cm or as small as 70 μm × 70 μm (10-μm diam-

eter spots may be achieved with very specialized equipment). It is applicable to biological, organic, and polymeric materials through metals, ceramics, and semiconductors. Smooth, flat samples are preferable but engineering samples and even powders can be handled. It is a nondestructive technique. Though there are some cases where the X-ray beam damage is significant (especially for organic materials), XPS is the least destructive of all the electron or ion spectroscopy techniques. It has relatively poor spatial resolution, compared to electron-impact and ion-impact techniques. It is also not suitable for trace analysis, the absolute sensitivity being between 0.01–0.3% at., depending on the element. XPS can be a slow technique if the extent of chemical detail to be extracted is large. Analysis times may vary from a few minutes to many hours.

There are thousands of commercial spectrometers in use today in materials analysis, chemistry, and physics laboratories. The largest concentrations are in the US and Japan. They are used in universities, the semiconductor and computer industries, and the oil, chemical, metallurgical, and pharmaceutical industries.

Instruments combining XPS with one or more additional surface techniques are not uncommon. Such combinations use up relatively little extra space but cost more.

Basic Principles

Background

A photon of sufficiently short wavelength (i.e., high energy) can ionize an atom, producing an ejected free electron. The kinetic energy KE of the electron (the photoelectron) depends on the energy of the photon $h\nu$ expressed by the Einstein photoelectric law:

$$KE = h\nu - BE \tag{1}$$

where BE is the binding energy of the particular electron to the atom concerned. All of photoelectron spectroscopy is based on Equation (1). Since $h\nu$ is known, a measurement of KE determines BE. The usefulness of determining BE for materials analysis is obvious when we remember the way in which the electron shells of an atom are built up. The number of electrons in a neutral atom equals the number of protons in the nucleus. The electrons, arranged in orbitals around the nucleus, are bound to the nucleus by electrostatic attraction. Only two electrons, of opposite spin, may occupy each orbital. The energy levels (or eigenvalues ε) of each orbital are discrete and are different for the same orbital in different atoms because the electrostatic attraction to the different nuclei (i.e., to a different number of protons) is different. To a first approximation, the BE of an electron, as determined by the amount of energy required to remove it from the atom, is equal to the ε value (this would be exactly true if, when removing an electron, all the other electrons did not

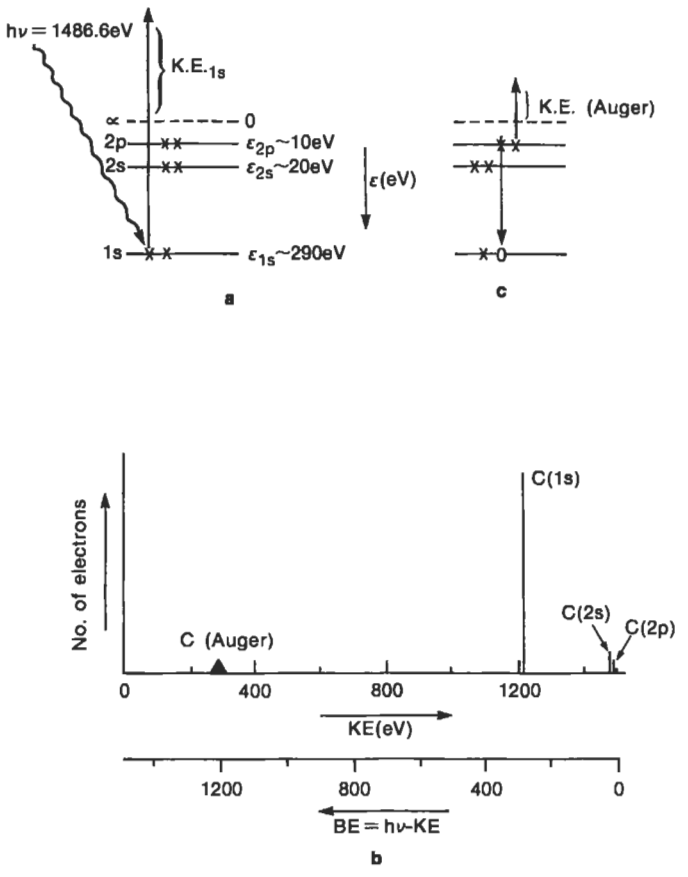

Figure 1 **(a) Schematic representation of the electronic energy levels of a C atom and the photoionization of a C 1s electron. (b) Schematic of the *KE* energy distribution of photoelectrons ejected from an ensemble of C atoms subjected to 1486.6-eV X rays.(c) Auger emission relaxation process for the C 1s hole-state produced in (a).**

respond in any way). So, by experimentally determining a *BE*, one is approximately determining an ε value, which is specific to the atom concerned, thereby identifying that atom.

Photoelectron Process and Spectrum

Consider what happens if, for example, an ensemble of carbon atoms is subjected to X rays of 1486.6 eV energy (the usual X-ray source in commercial XPS instruments). A carbon atom has 6 electrons, two each in the 1s, 2s, and 2p orbitals, usually written as C $1s^2\,2s^2\,2p^2$. The energy level diagram of Figure 1a represents this electronic structure. The photoelectron process for removing an electron from the

1s level, the most strongly bound level, is schematically shown. Alternatively, for any individual C atom, a 2s or a 2p electron might be removed. In an ensemble of C atoms, all three processes will occur, and three groups of photoelectrons with three different *KE*s will therefore be produced, as shown in Figure 1b where the *KE* distribution (the number of ejected photoelectrons versus the kinetic energy)—the photoelectron spectrum—is plotted. Using Equation (1), a *BE* scale can be substituted for the *KE* scale, and a direct experimental determination of the electronic energy levels in the carbon atom has been obtained. Notice that the peak intensities in Figure 1b are not identical because the probability for photoejection from each orbital (called the photoionization cross section, σ) is different. The probability also varies for a given orbital (e.g., a 1s orbital) in different atoms and depends on the X-ray energy used. For carbon atoms, using a 1486.6-eV X ray, the cross section for the 1s level, $\sigma_{C\,1s}$ is greater than $\sigma_{C\,2s}$ or $\sigma_{C\,2p}$, and therefore the C 1s XPS peak is largest, as in Figure 1b.

Thus, the number of peaks in the spectrum corresponds to the number of occupied energy levels in the atoms whose *BE*s are lower than the X-ray energy $h\nu$; the position of the peaks directly measures the *BE*s of the electrons in the orbitals and identifies the atom concerned; the intensities of the peaks depend on the number of atoms present and on the σ values for the orbital concerned. All these statements depend on the idea that electrons behave independently of each other. This is only an approximation. When the approximation breaks down, additional features can be created in the spectrum, owing to the involvement of some of the passive electrons (those not being photoejected).

Analysis Capabilities

Elemental Analysis

The electron energy levels of an atom can be divided into two types: core levels, which are tightly bound to the nucleus, and valence levels, which are only weakly bound. For the carbon atom of Figure 1, the C 1s level is a core level and the C 2s and 2p levels are valence levels. The valence levels of an atom are the ones that interact with the valence levels of other atoms to form chemical bonds in molecules and compounds. Their character and energy is changed markedly by this process, becoming characteristic of the new species formed. The study of these valence levels is the basis of ultraviolet photoelectron spectroscopy (UPS) discussed in another article in this encyclopedia. The core-level electrons of an atom have energies that are nearly independent of the chemical species in which the atom is bound, since they are not involved in the bonding process. Thus, in nickel carbide, the C 1s *BE* is within a few eV of its value for elemental carbon, and the Ni 2p *BE* is within a few eV of its value for Ni metal. The identification of core-level *BE*s thus provides unique signatures of the elements. All elements in the periodic table can be identified in this manner, except for H and He, which have no core levels. Approximate

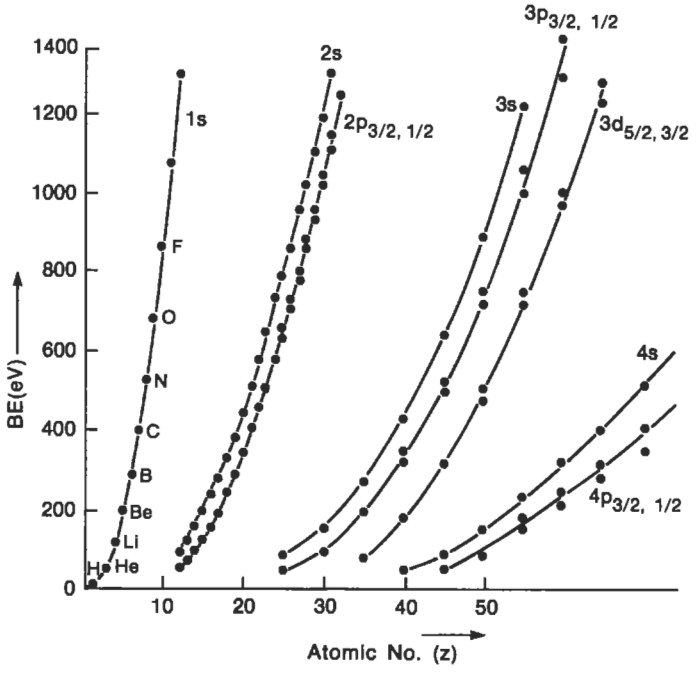

Figure 2 **Approximate *BE*s of the different electron shells as a function of atomic number *Z* of the atom concerned, up to the 1486.6-eV limit accessible by Al Kα radiation.** [2]

*BE*s of the electrons in all the elements in the period table up to $Z = 70$ are plotted in Figure 2, as a function of their atomic number Z, up to the usual 1486.6-eV accessibility limit.[2] Chance overlaps of *BE* values from core levels of different elements can usually be resolved by looking for other core levels of the element in doubt.

Quantitative analysis, yielding relative atomic concentrations, requires the measurement of relative peak intensities, combined with a knowledge of σ, plus any experimental artifacts that affect intensities. Cross section values are known from well-established calculations,[3] or from experimental measurements of relative peak areas on materials of known composition (standards).[4] A more practical problem is in correctly determining the experimental peak areas owing to variations in peak widths and line shapes, the presence of subsidiary features (often caused by the breakdown of the independent electron model), and the difficulty of correctly subtracting a large background in the case of solids. There are also instrumental effects to account for because electrons of different *KE* are not transmitted with equal efficiency through the electron energy analyzer. This is best dealt with by calibrating the instrument using local standards, i.e., measuring relative peak areas for stan-

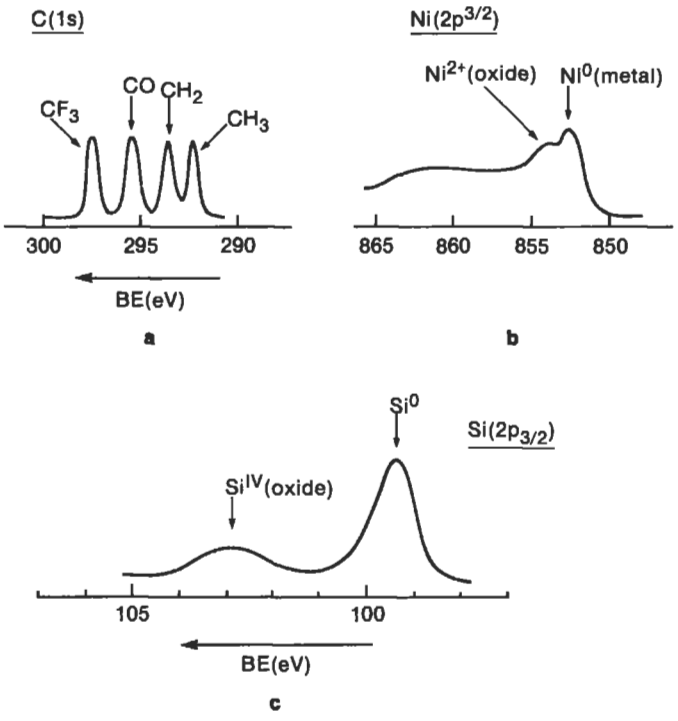

Figure 3 **(a) C 1s XPS spectrum from gaseous $CF_3COCH_2CH_3$. (b) Ni $2p_{3/2}$ XPS spectrum from a mixed Ni metal/Ni metal oxide system. (c) Si $2p_{3/2}$ XPS spectrum from a mixed Si/SiO_2 system.**

dards of known composition in the same instrument to be used for the samples of unknown composition. Taking all the above into account, the uncertainty in quantification in XPS can vary from a few percent in favorable cases to as high as 30% for others. Practitioners generally know which core levels and which types of materials are the most reliable, and in general, relative differences in composition of closely related samples can be determined with much greater accuracy than absolute compositions.

Chemical State Analysis

Though a core level *BE* is approximately constant for an atom in different chemical environments, it is not exactly constant. Figure 3a shows the C 1s part of the XPS spectrum of the molecule $CF_3COCH_2CH_3$. Four separated peaks corresponding to the four inequivalent carbon atoms are present.[1] The chemical shift range ΔBE covering the four peaks is about 8 eV compared to the *BE* of ~290 eV, or ~3%. The carbon atom with the highest positive charge on it, the carbon of the CF_3 group, has the highest *BE*. This trend of high positive charge and high *BE* is in accordance

Element	Oxidation state	Chemical shift from zero-valent state
Ni	Ni^{2+}	~2.2 eV
Fe	Fe^{2+}	~3.0 eV
	Fe^{3+}	~4.1 eV
Ti	Ti^{4+}	~6.0 eV
Si	Si^{4+}	~4.0 eV
Al	Al^{3+}	~2.0 eV
Cu	Cu^{+}	~0.0 eV
	Cu^{2+}	~1.5 eV
Zn	Zn^{2+}	~0 eV
W	W^{4+}	2 eV
	W^{6+}	4 eV

Table 1 **Typical chemical shift values for XPS core levels.**

with the simplest classical electrostatic representation of the atom as a sphere of radius r with a valence charge q on its surface. The potential inside the sphere q/r is felt by the 1s electrons. If q increases, the *BE* of the 1s level increases, and vice versa. This picture is a gross oversimplification because electrons are not so well separated in space, but the general idea that the *BE* increases with increasing charge on the atom holds in the majority of cases. Table 1 lists the approximate chemical shifts found for the different oxidation states of various metals and semiconductors. The typical range is 1 to several eV, though in some important cases (e.g., Cu and Zn) it is very small. Typical spectra illustrating these chemical shifts for a mixed Ni metal/nickel oxide system and a mixed silicon/silicon dioxide system are shown in Figures 3b and 3c.

The spectra of Figure 3 illustrate two further points. All the C 1s peaks in Figure 3a are of equal intensity because there are an equal number of each type of C atom present. So, when comparing relative intensities of the same atomic core level to get composition data, we do not need to consider the photoionization cross section. Therefore, Figure 3c immediately reveals that there is four times as much elemental Si present as SiO_2 in the Si 2p spectrum. The second point is that the chemical shift range is poor compared to the widths of the peaks, especially for the solids in Figures 3b and 3c. Thus, not all chemically inequivalent atoms can be distin-

guished this way. For example, Cu^0 (metal) is not distinguishable from Cu^+ in Cu_2O, and Zn^0 is not distinguishable from Zn^{2+} (e.g., in ZnO).

More Complex Effects

In reality, while the photoelectron is leaving the atom, the other electrons respond to the hole being created. The responses, known as *final state effects*, often lead to additional features in the XPS spectrum, some of which are useful analytically.

An effect that always occurs is a lowering of the total energy of the ion due to the relaxation of the remaining electrons towards the hole. This allows the outgoing photoelectron to carry away greater *KE*, i.e., the *BE* determined is always lower than ε. This needs to be considered when comparing theoretical ε values to experimental *BE*s, i.e., for detailed interpretation of electronic structure effects, but is not generally used analytically.

Spin–orbit splitting results from a coupling of the spin of the unpaired electron left behind in the orbital from which its partner has been photoejected with the angular momentum of that orbital, giving two possible different energy final states (spin up or spin down). It occurs for all levels except s levels, which have no orbital angular momentum (being spherical), turning single peaks into doublet peaks. The splitting increases with *Z*, as can be seen from Figure 2 in, for example, the $2p_{3/2}$ and $2p_{1/2}$ spin–orbit split components of the 2p level. The only analytical usefulness is that the splitting increases the number of XPS peaks per atom in a completely known way, which can help when overlaps occur.

Some elements, particularly the transition metals, have unpaired electron spins in their valence levels. The degree of unpairing is strongly affected by the bonding process to other atoms. An unpaired core-electron remaining after the photoemission process will couple to any unpaired spin in the valence level, again leading to more than one final state and peak splitting, called multiplet splitting (weaker than the equivalent spin-orbital splitting). Since the degree of unpaired electron spin in the valence levels is strongly affected by chemical bonding, so is the size of the multiplet splitting. For example, the Cr (3s) level of the Cr^{III} ion of Cr_2O_3 is split by 4.2 eV, whereas in the more covalent compound Cr_2S_3 the splitting is 3.2 eV, allowing distinction of Cr^{III} in the two compounds.[5]

While a core-electron is being ejected, there is some probability that a valence electron will be simultaneously excited to an empty orbital level during the relaxation process, Figure 4b. If this shake-up process occurs, the photoelectron must be ejected with less energy, shifting the XPS peak to apparently higher *BE* than for a case where shake-up doesn't occur, as shown in Figure 4c. These "shake-up satellites" in the spectrum are usually weak because the probability of their occurrence is low, but in some cases they can become as strong as the "main" peak. Shake-up structure can provide chemical state identification because the valence levels are involved. A typical example is given in Figure 4d. The ion Cu^{2+} (in CuO) is distin-

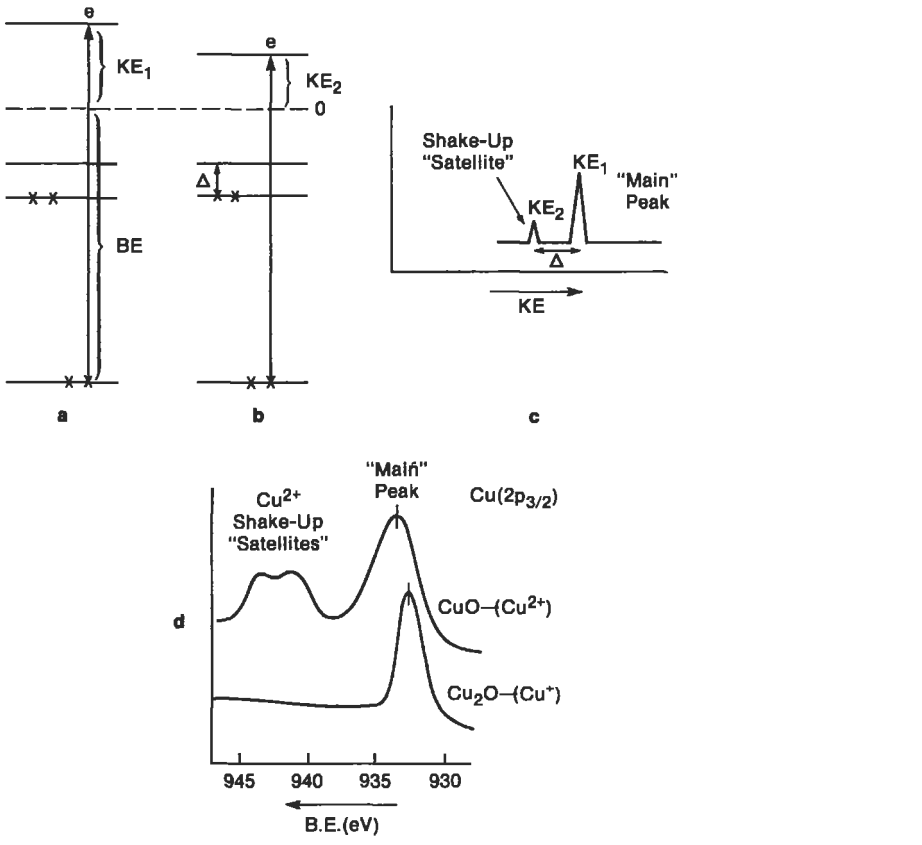

Figure 4 **Schematic electron energy level diagram: (a) of a core-level photoelectron ejection process (one electron process); (b) core-level photoelectron ejection process with shake-up (two- electron process); (c) schematic XPS spectrum from (a) plus (b); (d) Cu $2p_{3/2}$ XPS spectrum for Cu^+ in Cu_2O and Cu^{2+} in CuO. The latter shows strong shake-up features.**

guishable from Cu^+ (in Cu_2O) by the presence of the very characteristic strong Cu 2p shake-up structure for Cu^{2+}. The chemical shift between Cu^{2+} and Cu^+ could also be used for identification, provided accurate *BE*s are measured. It is sometimes an advantage not to have to rely on accurate *BE*s, for instance, when comparing data of different laboratories or if there is a problem establishing an accurate value because of sample charging. In such cases the "fingerprinting" pattern identification of a main peak plus its satellites, as in Figure 4d, is particularly useful.

After the photoemission process is over, the core-hole left behind can eventually be filled by an electron dropping into it from another orbital, as shown in Figure 1c for the example of carbon. The energy released, in this example $\varepsilon_{1s} - \varepsilon_{2p}$, may be

sufficient to eject another electron. The example of a 2p electron being ejected is shown. This is called Auger electron emission and the approximate *KE* of the ejected Auger electron will be

$$KE(\text{Auger}) = (\varepsilon_{1s} - \varepsilon_{2p}) - \varepsilon_{2p} \tag{2}$$

The value is characteristic of the atomic energy levels involved and, therefore, also provides a direct element identification (see the article on AES). The *KE* (Auger) is independent of the X-ray energy $h\nu$ and therefore it is not necessary to use monochromatic X rays to perform Auger spectroscopy. Therefore, the usual way Auger spectroscopy is performed is to use high- energy electron beams to make the core-holes, as discussed in the AES article. We mention the process here, however, because when doing XPS the allowable Auger process peaks are superimposed on the spectrum, and they can be used as an additional means of element analysis. Also, in many cases, chemical shifts of Auger peaks, which have a similar origin to XPS core-level shifts, are larger, allowing chemical state identification in cases where it is not possible directly from the XPS core levels. For example, Zn^{2+} can be distinguished from Zn^0 by a 3-eV shift in Auger peak *KE*, whereas it was mentioned earlier that the two species were not distinguishable using XPS core levels.

Surface Sensitivity

Electrons in XPS can travel only short distances through solids before losing energy in collisions with atoms. This inelastic scattering process, shown schematically in Figure 5a, is the reason for the surface sensitivity of XPS. Photoelectrons ejected from atoms "very near" the surface escape unscattered and appear in the XPS peaks. Electrons originating from deeper have correspondingly reduced chances of escaping unscattered and mostly end up in the background at lower *KE* after the XPS peak, as in Figure 5b. Thus, the peaks come mostly from atoms near the surface, the background mostly from the bulk.

If I_0 is the flux of electrons originating at depth d, the flux emerging without being scattered, I_d, exponentially decreases with depth according to

$$I_d = I_0^{\frac{-d}{\lambda_e \sin\theta}} \tag{3}$$

where θ is the angle of electron emission and $d/\sin\theta$ is the distance travelled through the solid at that angle. The quantity λ_e is called the *inelastic mean free path length*. The value of λ_e, which determines quantitatively exactly how surface sensitive the measurement is, depends on the *KE* of the electron and the material through which it travels. Empirical relationships between λ_e and *KE* are plotted in Figure 6 for elements and for compounds.[6] They are meant as rough guides because values can vary considerably (by a factor of almost 4), depending on what element

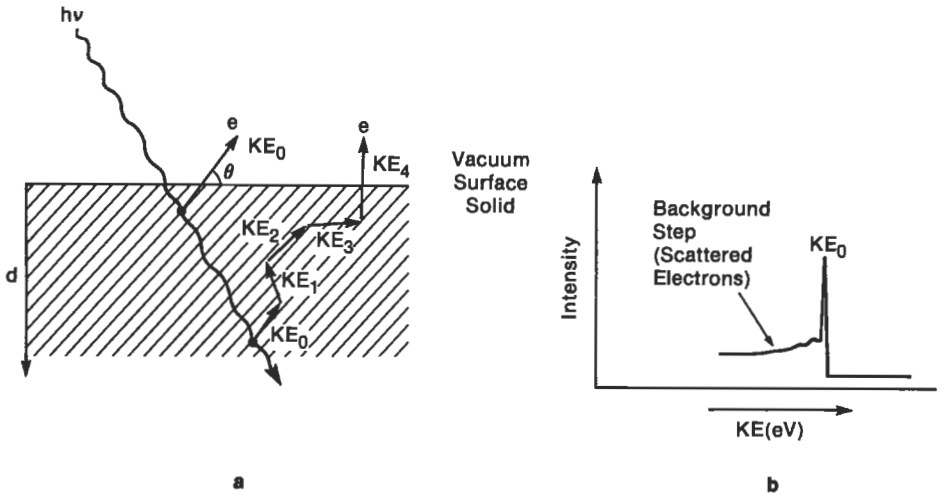

Figure 5 **(a) Schematic of inelastic electron scattering occurring as a photoelectron, initial energy KE_0, tries to escape the solid, starting at different depths. $KE_4 < KE_3 < KE_2 < KE_1 < KE_0$. (b) *KE* energy distribution (i.e., electron spectrum) obtained due to the inelastic scattering in (a). Note that the peak, at E_0, must come mainly from the surface region, and the background step, consisting of the lower energy scattered electrons, from the bulk.**

or compound is involved. Substituting λ_e values from the curves into Equation (3) tells us that for normal emission ($\theta = 90°$) using a 200-eV *KE* XPS peak, 90% of the signal originates from the top ~25 Å, for elements. For a 1400-eV peak the depth is ~60 Å. The numbers are about twice as big for compounds. Thus, the depth probed by XPS varies strongly depending on the XPS peaks used and the material involved. The depth probed can also be made smaller for any given XPS peak and material by detecting at grazing emission angle θ. For smooth surfaces, values down to 10° are practical, for which the depth probed is reduced by a factor of 1/sin 10, or ~6, compared to 90°, from Equation (3). Varying *KE* or θ are important practical ways of distinguishing what is in the outermost atomic layers from what is underneath.

Instrumentation

An XPS spectrometer schematic is shown in Figure 7. The X-ray source is usually an Al- or Mg-coated anode struck by electrons from a high voltage (10–15 kV) Alkα or Mgkα radiation lines produced at energies of 1486.6 eV and 1256.6 eV, with line widths of about 1 eV. The X rays flood a large area (~1 cm^2). The beam's spot size can be improved to about 100-μm diameter by focusing the electron beam

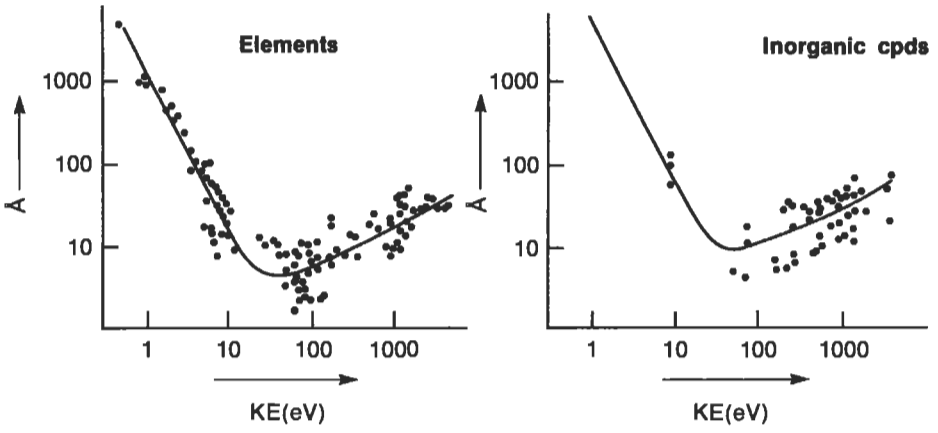

Figure 6 **Mean free path lengths λ_e as a function of *KE*, determined for (a) metals and (b) inorganic compounds.[6]**

onto the anode and passing the X rays through an X-ray monochromator. The latter also improves line widths to between 0.5 and 0.25 eV, leading to higher resolution spectra (thus improving the chemical state identification process) and removing an unwanted X-ray background at lower energies.

Practical limits to the shape and size of samples are set by commercial equipment design. Some will take only small samples (e.g., 1 cm × 1 cm) while others can handle whole 8-in computer disks. Flat samples improve signal strength and allow quantitative θ variation, but rough samples and powders are also routinely handled. Insulating samples may charge under the X-ray beam, resulting in inaccurate *BE* determinations or spectra distorted beyond use. The problem can usually be mitigated by use of a low-energy electron flood gun to neutralize the charge, provided this does not damage the sample.

The electron lenses slow the electrons before entering the analyzer, improving energy resolution. They are also used to define an analyzed area on the sample from which electrons are received into the analyzer and, in one commercial design, to image the sample through the analyzer with 10-μm resolution. Older instruments may have slits instead of lenses. The most popular analyzer is the hemispherical sector, which consists of two concentric hemispheres with a voltage applied between them. This type of analyzer is naturally suited to varying θ by rotating the sample, Figure 7. The XPS spectrum is produced by varying the voltages on the lenses and the analyzer so that the trajectories of electrons ejected from the sample at different energies are brought, in turn, to a focus at the analyzer exit slit. A channeltron type electron multiplier behind the exit slit of the analyzer amplifiers individual electrons by 10^5–10^6, and each such pulse is fed to external conventional pulse counting electronics and on into a computer. The computer also controls the lens and

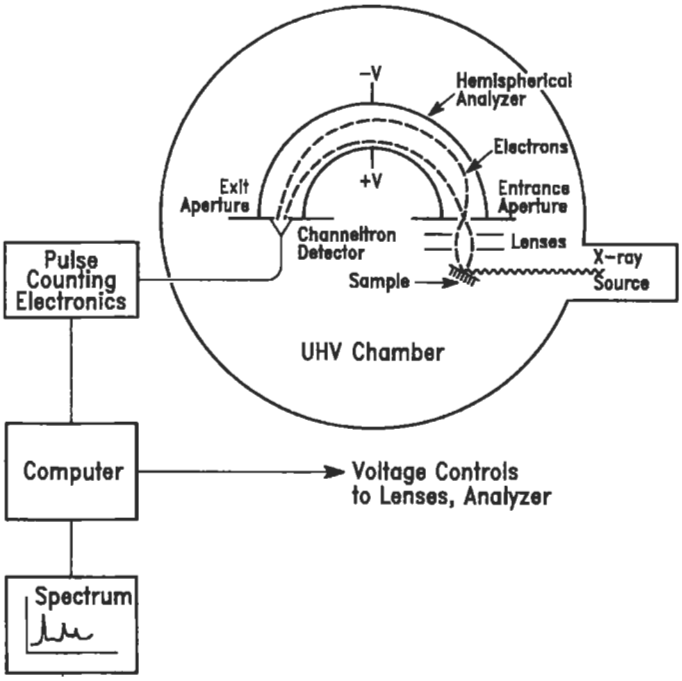

Figure 7 **Schematic of a typical electron spectrometer showing all the necessary components. A hemispherical electrostatic electron energy analyser is depicted.**

analyzer voltages. A plot of electron pulses counted against analyzer–lens voltage gives the photoelectron spectrum. More sophisticated detection schemes replace the exit slit–multiplier arrangement with a multichannel array detector. This is the modern equivalent of a photographic plate, allowing simultaneous detection of a range of *KE*s, thereby speeding up the detection procedure.

Commercial spectrometers are usually bakeable, can reach ultrahigh-vacuum pressures of better than 10^{-9} Torr, and have fast-entry load-lock systems for inserting samples. The reason for the ultrahigh-vacuum design, which increases cost considerably, is that reactive surfaces, e.g., clean metals, contaminate rapidly in poor vacuum (1 atomic layer in 1 s at 10^{-6} Torr). If the purpose of the spectrometer is to always look at as-inserted samples, which are already contaminated, or to examine rather unreactive surfaces (e.g., polymers) vacuum conditions can be relaxed considerably.

Applications

XPS is routinely used in industry and research whenever elemental or chemical state analysis is needed at surfaces and interfaces and the spatial resolution requirements are not demanding (greater than 150 μm). If the analysis is related specifically to the top 10 or so atomic layers of air-exposed sample, the sample is simply inserted and data taken. Examples where this might be appropriate include: examination for and identification of surface contaminants; evaluation of materials processing steps, such as cleaning procedures, plasma etching, thermal oxidation, silicide thin-film formation; evaluation of thin-film coatings or lubricants (thickness–quantity, chemical composition); failure analysis for adhesion between components, air oxidation, corrosion, or other environmental degradation problems, tribological (wear) activity; effectiveness of surface treatments of polymers and plastics; surface composition differences for alloys; examination of catalyst surfaces before and after use, after "activation" procedures, and unexplained failures.

Figure 3c was used to illustrate that Si^{IV} could be distinguished from Si^0 by the Si 2p chemical shift. The spectrum is actually appropriate for an oxidized Si wafer having an ~10-Å SiO_2 overlayer. That the SiO_2 is an overlayer can easily be proved by decreasing θ to increase the surface sensitivity; the Si^0 signal will decrease relative to the Si^{IV} signal. The 10-Å thickness can be determined from the Si^{IV}/Si^0 ratio and Equation (3), using the appropriate λ_e value. That the overlayer is SiO_2 and not some other Si^{IV} compound is easily verified by observing the correct position (*BE*) and intensity of the O 1s peak plus the absence of other element peaks. If the sample has been exposed to moisture, including laboratory air, the outermost atomic layer will actually be hydroxide, not oxide. This is easily recognized since there is a chemical shift between OH and O in the O 1s peak position.

Figure 8 shows a typical example where surface modification to a polymer can be followed.[7] High-density polyethylene $(CH_2CH_2)_n$ was surface-fluorinated in a dilute fluorine–nitrogen mixture. Spectrum A was obtained after only 0.5 s treatment. A F 1s signal corresponding to about a monolayer has appeared, and CF formation is obvious from the chemically shifted shoulder on the C 1s peak at the standard CF position. After 30 s reaction, the F 1s / C 1s ratio indicates (spectrum B) that the reaction has proceeded to about 30 Å depth, and that CF_2 formation has occurred, judging by the appearance of the C 1s peak at 291 eV. Angular studies and more detailed line shape and relative intensity analysis, compared to standards, showed that for the 0.5-s case, the top monolayer is mainly polyvinyl fluoride $(CFHCH_2)_n$, whereas after 30 s polytrifluoroethylene $(CF_2CFH)_n$ dominates in the top two layers. While this is a rather aggressive example of surface treatment of polymers, similar types of modifications frequently are studied using XPS. An equivalent example in the semiconductor area would be the etching processes of Si/SiO_2 in CF_4/O_2 mixtures, where varying the CF_4/O_2 ratio changes the relative etching rates of Si and SiO_2, and also produces different and varying amounts of residues at the wafer's surface.

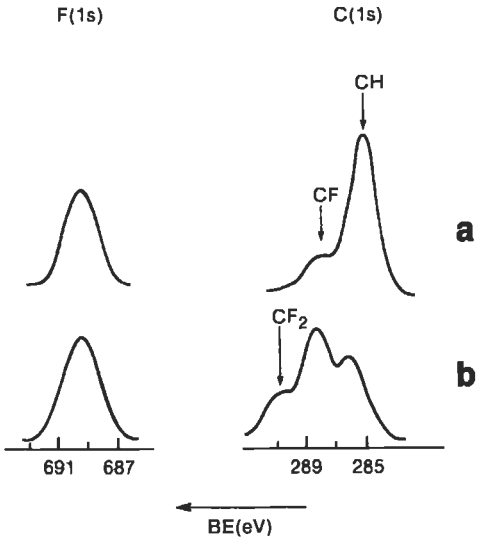

Figure 8 **XPS spectrum in the C 1s and F 1s regions of polyethylene $(CH_2)_n$, treated with a dilute F_2/N_2 gaseous mixture for (a) 0.5 sec, and (b) 30 sec.[7]**

In many applications the problem or property concerned is not related just to the top 10 or so atomic layers. Information from deeper regions is required for a number of reasons: A thick contaminant layer, caused by air exposure, may have covered up the surface of interest; the material may be a layered structure in which the buried interfaces are important; the composition modulation with depth may be important, etc. In such cases, the 2–15 atomic layer depth resolution attainable in XPS by varying θ is insufficient, and some physical means of stripping the surface while taking data, or prior to taking data, is required. This problem is common to all very surface sensitive spectroscopies. The most widely used method is argon ion sputtering, done inside the spectrometer while taking data. It can be used to depths of μm, but is most effective and generally used over much shorter distances (hundreds and thousands of Å) because it can be a slow process and because sputtering introduces artifacts that get worse as the sputtered depth increases.[8] These include interfacial mixing caused by the movement of atoms under the Ar^+ beam, elemental composition alteration caused by preferential sputtering of one element versus another, and chemical changes caused by bonds being broken by the sputtering process.

If the interface or depth of interest is beyond the capability of sputtering, one can try polishing down, sectioning, or chemical etching the sample before insertion.

The effectiveness of this approach varies enormously, depending on the material, as does the extent of the damaged region left at the surface after this preparation treatment.

In some cases, the problem or property of interest can be addressed only by performing experiments inside the spectrometer. For instance, metallic or alloy embrittlement can be studied by fracturing samples in ultrahigh vacuum so that the fractured sample surface, which may reveal why the fracture occurred in that region, can be examined without air exposure. Another example is the simulation of processing steps where exposure to air does not occur, such as many vacuum deposition steps in the semiconductor and thin-film industries. Studying the progressive effects of oxidation on metals or alloys inside the spectrometer is a fairly well-established procedure and even electrochemical cells are now coupled to XPS systems to examine electrode surfaces without air exposure. Sometimes materials being processed can be capped by deposition of inert material in the processing equipment (e.g., Ag, Au, or in GaAs work, arsenic oxide), which is then removed again by sputtering or heating after transfer to the XPS spectrometer. Finally, attempts are sometimes made to use "vacuum transfer suitcases" to avoid air exposure during transfer.

Comparison with other Techniques

XPS, AES, and SIMS are the three dominant surface analysis techniques. XPS and AES are quite similar in depth probed, elemental analysis capabilities, and absolute sensitivity. The main XPS advantages are its more developed chemical state analysis capability, somewhat more accurate elemental analysis, and far fewer problems with induced sample damage and charging effects for insulators. AES has the advantage of much higher spatial resolutions (hundreds of Å compared to tens of μm), and speed. Neither is good at trace analysis, which is one of the strengths of SIMS (and related techniques). SIMS also detects H, which neither AES nor XPS do, and probes even less deeply at the surface, but is an intrinsically destructive technique. Spatial resolution is intermediate between AES and XPS. ISS is the fourth spectroscopy generally considered in the "true surface analysis" category. It is much less used, partly owing to lack of commercial instrumentation, but mainly because it is limited to elemental analysis with rather poor spectral distinction between some elements. It is, however, the most surface sensitive elemental analysis technique, seeing only the top atomic layer. With the exception of EELS and HREELS, all other spectroscopies used for surface analysis are much less surface sensitive than the above four. HREELS is a vibrational technique supplying chemical functional group information, not elemental analysis, and EELS is a rarely used and specialized technique, which, however, can detect hydrogen.

Conclusions

XPS has developed into the most generally used of the truly surface sensitive techniques, being applied now routinely for elemental and chemical state analysis over a range of materials in a wide variety of technological and chemical industries. Its main current limitations are the lack of high spatial resolutions and relatively poor absolute sensitivity (i.e., it is not a trace element analysis technique). Recently introduced advances in commercial equipment have improved speed and sensitivity by using rotating anode X-ray sources (more photons) and parallel detection schemes. Spot sizes have been reduced from about 150 μm, where they have languished for several years, to 75 μm. Spot sizes of 10 μm have been achieved, and recently anounced commercial instruments offer these capabilities. When used in conjunction with focused synchrotron radiation in various "photoelectron microscope" modes higher resolution is obtainable. Routinely available 1 μm XPS resolution in laboratory-based equipment would be a major breakthrough, and should be expected within the next three years.

Special, fully automated one-task XPS instruments are beginning to appear and will find their way into both quality control laboratories and process control on production lines before long.

More detailed discussions of XPS can be found in references 4–12, which encompass some of the major reference texts in this area.

Related Articles in the Encyclopedia

UPS, AES, SIMS, and ISS

References

1 K. Siegbahn et al. *ESCA: Atomic, Molecular, and Solid State Structure Studied by Means of Electron Spectroscopy.* Nova Acta Regime Soc. Sci., Upsaliensis, 1967, Series IV, Volume 20; and K. Siegbahn et al. *ESCA Applied to Free Molecules.* North Holland, Amsterdam, 1969. These two volumes, which cover the pioneering work of K.Siegbahn and coworkers in developing and applying XPS, are primarily concerned with chemical structure identification of molecular materials and do not specifically address surface analysis.

2 Charts such as this, but in more detail, are provided by all the XPS instrument manufacturers. They are based on extensive collections of data, much of which comes from Reference 1.

3 J. H. Scofield. *J. Electron Spect.* **8,** 129, 1976. This is the standard quoted reference for photoionization cross sections at 1487 eV. It is actually one of the most heavily cited references in physical science. The calculations are published in tabular form for all electron level of all elements.

See, for example, S. Evans et al. *J. Electr. Spectr.* **14,** 341, 1978. Relative experimental ratios of cross sections for the most intense peaks of most elements are given.

5 J. C. Carver, G. K. Schweitzer, and T. A. Carlson. *J. Chem. Phys.* **57,** 973, 1972. This paper deals with multiplet splitting effects, and their use in distinguishing different element states, in transition metal complexes.

6 M. P. Seah and W. A. Dench. *Surf. Interface Anal.* **1,** 1, 1979. Of the many compilations of measured mean free path length versus *KE*, this is the most thorough, readable, and useful.

7 D. T. Clark, W. J. Feast, W. K. R. Musgrave, and I. Ritchie. *J. Polym. Sci. Polym. Chem.* **13,** 857, 1975. One of many papers from Clark's group of this era which deal with all aspects of XPS of polymers.

8 See the article on surface roughness in Chapter 12.

9 The book series *Electron Spectroscopy: Theory, Techniques, and Applications*, edited by C. R. Brundle and A. D. Baker, published by Academic Press has a number of chapters in its 5 volumes which are useful for those wanting to learn about the analytical use of XPS: In Volume 1, *An Introduction to Electron Spectroscopy* (Baker and Brundle); in Volume 2, *Basic Concepts of XPS* (Fadley); in Volume 3, *Analytical Applications of XPS* (Briggs); and in Volume 4, *XPS for the Investigation of Polymeric Materials* (Dilks).

10 T. A. Carlson, *Photoelectron and Auger Spectroscopy*, Plenum, 1975. A complete and largely readable treatment of both subjects.

11 *Practical Surface Analysis*, edited by D. Briggs and M. P. Seah, published by J. Wiley; *Handbook of XPS and UPS*, edited by D. Briggs. Both contain extensive discussion on use of XPS for surface and material analysis.

12 *Handbook of XPS*, C. D. Wagner, published by PHI (Perkin Elmer). This is a book of XPS data, invaluable as a standard reference source.

5.2 UPS

Ultraviolet Photoelectron Spectroscopy

C. R. BRUNDLE

Contents

Introduction

The photoelectric process, which was discovered in the early 1900s, was developed as a means of studying the electronic structure of molecules in the gas phase in the early 1960s, largely owing to the pioneering work of D. W. Turner's group.[1] A major step was the introduction of the He resonance discharge lamp as a laboratory photon source, which provides monochromatic 21.2-eV light. In conjunction with the introduction of high resolution electron energy analyzers, this enables the binding energies (BE) of all the electron energy levels below 21.2 eV to be accurately determined with sufficient spectral resolution to resolve even vibrational excitations. Coupled with theoretical calculations, these measurements provide information on the bonding characteristics of the valence-level electrons that hold molecules together. The area has become known as ultraviolet photoelectron spectroscopy (UPS) because the photon energies used (21.2 eV and lower) are in the vacuum ultraviolet (UV) part of the light spectrum. It is also known as molecular photoelectron spectroscopy, because of its ability to provide molecular bonding information.

In parallel with these developments for studying molecules, the same technique was being developed independently to study solids; particularly metals and semi-

conductors.[2] This branch of the technique is usually known as UV photoemission. Here the electronic structure of the solid (the band structure for metals and semiconductors) was the interest. Since the technique is sensitive to only the top few atomic layers, the electronic structure of the surface, which in general can be different from that of the bulk, is actually obtained. The two branches of UPS, gas-phase and solid-surface studies, come together when adsorption and reaction of molecules at surfaces is studied.[3,4]

Though commercial UPS instruments were sold in the 1970s, for gas-phase work, none are sold today. Since the only additional item required to perform UPS on an XPS instrument is a He source, this is usually how UPS is performed in the laboratory. An alternative, more specialized approach, is to couple an electron spectrometer to the beam-line monochromator of a synchrotron facility. This provides a tunable source of light, usually between around 10 eV and 200 eV, though many beam lines can obtain much higher energies. This approach can provide a number of advantages, including variable surface sensitivity and access to core levels up to the photon energy used, at much higher resolution than obtainable by laboratory XPS instruments. Even using a laboratory UPS source, such as a He resonance lamp, some low-lying core levels are accessible. When using either synchrotron or laboratory sources to access core levels, all the materials surface analysis capabilities of XPS described in the preceding article become available.

Basic Principles

The photoionization process and the way it is used to measure BEs of electrons to atoms is described in the article on XPS and will not be repeated here. Instead, we will concentrate on the differences between the characteristics of core-level BEs, described in the XPS article, and those of valence-level BEs. In Figure 1a the electron energy-level diagram for a CO molecule is shown, schematically illustrating how the atomic levels of the C and O atom interact to form the CO molecule. The important point to note is that whereas the BEs of the C 1s and O 1s core levels remain characteristic of the atoms when the CO molecule is formed (the basis of the use of XPS as an elemental analysis tool), the C 2p and O 2p valence levels are no longer characteristic of the individual atoms, but have combined to form a new set of molecular orbitals entirely characteristic of the CO molecule. Therefore, the UPS valence-band spectrum of the CO molecule, Figure 1b, is also entirely characteristic of the molecule, the individual presence of a C atom and an O atom no longer being recognizable. For a solid, such as metallic Ni, the valence-level electrons are smeared out into a band, as can be seen in the UPS spectrum of Ni (Figure 2a). For molecules adsorbed on surfaces there is also a smearing out of structure. For example, Figure 2b shows a monolayer of CO adsorbed on an Ni surface.

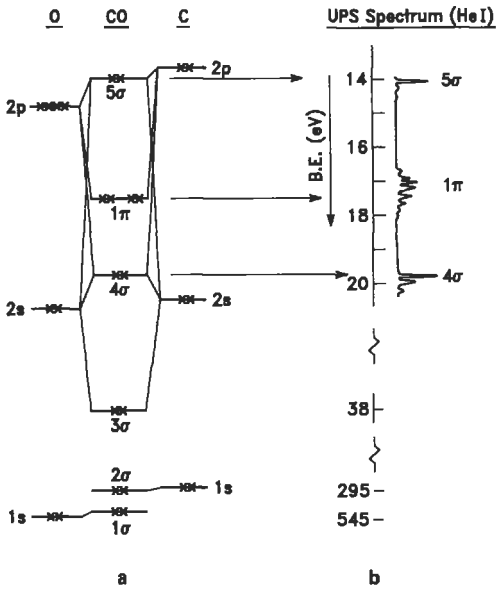

Figure 1 **(a) Electron energy diagram for the CO molecule, illustrating how the molecular orbitals are constructed from the atomic levels. (b) He I UPS spectrum of CO.[1]**

Analytical Capabilities

As stated earlier, the major use of UPS is not for materials analysis purposes but for electronic structure studies. There are analysis capabilities, however. We will consider these in two parts: those involving the electron valence energy levels and those involving low-lying core levels accessible to UPS photon energies (including synchrotron sources). Then we will answer the question "why use UPS if XPS is available?"

Valence Levels

The spectrum of Figure 1b is a fingerprint of the presence of a CO molecule, since it is different in detail from that of any other molecule. UPS can therefore be used to identify molecules, either in the gas phase or present at surfaces, provided a data bank of molecular spectra is available, and provided that the spectral features are sufficiently well resolved to distinguish between molecules. By now the gas phase spectra of most molecules have been recorded and can be found in the literature.[1, 5] Since one is using a pattern of peaks spread over only a few eV for identification purposes, mixtures of molecules present will produce overlapping patterns. How well mixtures can be analyzed depends, obviously, on how well overlapping peaks can be resolved. For molecules with well-resolved fine structure (vibrational) in the spectra (see Figure 1b), this can be done much more successfully than for the broad,

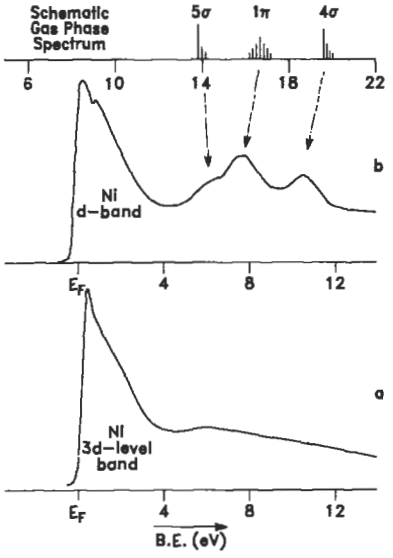

Figure 2 **(a) He II UPS spectrum of a Ni surface.[4] (b) He II UPS spectrum of a CO monolayer adsorbed on a Ni surface.[4] Note the broadening and relative binding-energy changes of the CO levels compared to the gas phase spectrum. Gas-phase binding energies were measured with respect to the vacuum level; solid state binding energies relative to the Fermi level E_F.**

unresolved bands found for solid surfaces (see Figure 2b). For solids that have electronic structure characteristics in between those of molecules and metals, such as polymers, ionic compounds, or molecules adsorbed on surfaces (Figure 2b), enough of the individual molecular-like structure of the spectra often remains for the valence levels to be used for fingerprinting purposes. Reactions between molecules and surfaces often can be fingerprinted also. For example, in Figure 3 the UPS differences between molecular H_2O on a metal, and its only possible dissociation fragments, OH and atomic O, are schematically illustrated.

The examples of valence-level spectra given so far, for solid surfaces, i.e., those in Figures 2a, 2b, and 3, are all *angle-integrated* spectra; that is, electrons emitted over a wide solid angle of emission are collected and displayed. In fact, the energy distribution of photoemitted electrons from solids varies somewhat depending on the direction of emission and if data is taken in an angular-resolved mode, that is, for specific directions for the photon beam and the photoemitted electrons, detailed information about the three-dimensional (3D) band structure of the solid, or the two-dimensional (2D) band structure of an adsorbate overlayer may be obtained, together with information on the geometric orientation of such adsorbate mole-

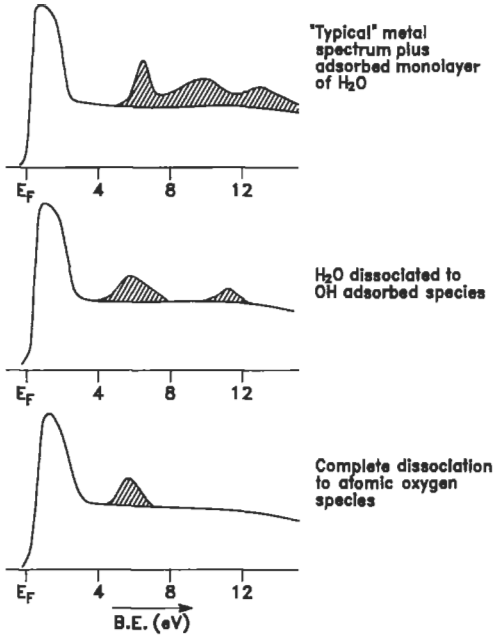

Figure 3 **Schematic spectra of H_2O, OH, and atomic O adsorbed on a metal surface illustrate how molecules can be distinguished from their reactor products by fingerprinting.**

cules. To properly exploit the technique requires also variation of the photon energy, $h\nu$ (therefore requiring synchrotron radiation) and the polarization of the radiation (s and p, naturally available from the synchrotron source). Basically, recording the UPS spectrum while varying all these parameters (angle, photon energy, and polarization) picks out specific parts of the density of states. A fuller description of this type of work[6] is beyond the scope of this article and is not particularly relevant to materials analysis, except for the fact that molecular orientation at surfaces can be determined. This property is, however, restricted to situations with long-range order, i.e., 2D arrays of molecules on single-crystal surfaces.

Low-Lying Accessible Core Levels

Table 1 lists core levels and their BEs for elements commonly used in technology, which are sufficiently sharp and intense, and which are accessible to laboratory He I or He II sources (21.2-eV or 40.8-eV photon energy) or to synchrotron sources (up to 200 eV or higher). The analytical approaches are the same as described in the XPS article. For example, in that article examples were given of Si 2p spectra obtained using a laboratory Al Kα X-ray source at 1486-eV photon energy. The

Element	Core level	Approximate binding energy (eV)	Usable r radiation
Al	2p	72	S
Si	2p	100	S
S	2p	164	S
Zn	3d	9	He I, He II, S
Ga	3d	18	He I, He II, S
Ge	3d	29	He II, S
As	3d	41	S
Ta	4f	25	He II, S
W	4f	34	S
Ir	4f	60	S
Pt	4f	70	S
Au	4f	84	S
Hg	4f	99	S
	5d	7	He I, He II, S
Pb	4f	138	S

Table 1 **Narrow, intense core levels of some elements commonly used in technological materials that are accessible to He I/He II radiation, or synchrotron radiation below 200 eV.**

Si 2p line, at about 100 eV BE, is also easily accessible at most synchrotron sources but cannot, of course, be observed using He I and He II radiation. On the other hand, the Zn 3d and Hg 4f lines can be observed quite readily by He I radiation (see Table 1) and the elements identified in this way. Quantitative analysis using relative peak intensities is performed exactly as in XPS, but the photoionization cross sections σ are very different at UPS photon energies, compared to Al Kα energies, and tabulated or calculated values are not so readily available. Quantitation, therefore, usually has to be done using local standards.

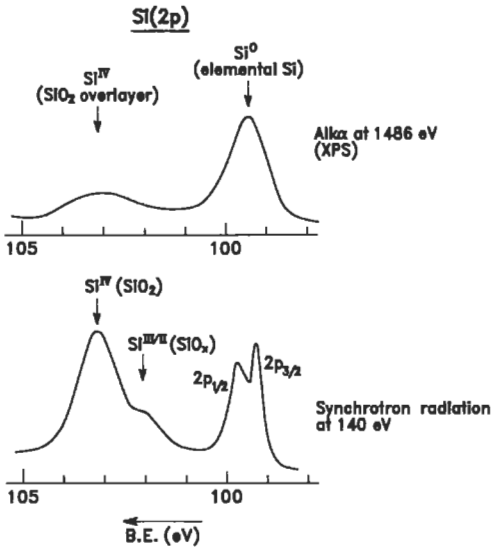

Figure 4 **Schematic comparison of the Si 2p spectra of an Si/SiO_2 interface taken using Al K radiation at 1486 eV and synchrotron radiation at 40 eV photon energy. Note the greater surface sensitivity and higher resolution in the synchrotron case.**

Why Use UPS for Analysis?

Since all the valence levels and core levels that are accessible to UPS photon sources are also accessible to XPS, what are the reasons for ever wanting to use laboratory He sources or synchrotron radiation? There are at least four significant differences that can be important analytically in special circumstances. First, the surface sensitivity is usually greater in UPS because for a given energy level being examined, the lower photon energy sources in UPS yield ejected photoelectrons having lower kinetic energies. For example, the Si 2p signal of Figure 3 in the XPS article consists of electrons having a kinetic energy 1486–100 eV = 1386 eV. If the Si 2p spectrum were recorded using 140 eV synchrotron photons, the kinetic energy would be 140–100 eV = 40 eV. Looking at the inelastic mean-free path length diagram of Figure 6 in the XPS article, one can see that 40-eV photoelectrons have about one-third the inelastic scattering length of 1400-eV electrons. Therefore the synchrotron recorded signal would be roughly three times as surface sensitive, as illustrated in Figure 4 where the XPS SiO_2 / Si spectrum is schematically compared for 1486 eV and 140 eV photon sources. The SiO_2 part of the Si 2p signal is much stronger in the synchrotron spectrum and therefore much thinner layers will be more easily detectable.

Secondly, spectral resolution can be significantly higher for UPS or synchrotron data, compared to XPS. This is simply a consequence of UPS (synchrotron) sources

having narrower line widths than laboratory X-ray sources. Thus, whereas the XPS recorded Si 2p signal of Figure 4 has a width of about 1 eV, the individual $2p_{3/2}$ and $2p_{1/2}$ components of the synchrotron recorded signal are only about 0.25 eV wide. Whether this resolution improvement can be achieved in any individual case depends on the natural line width of the particular core level concerned. Si 2p, W 4f, Al 2p, Pt 4f, and Au 4f are all examples of narrow core lines, where a large resolution improvement would occur using synchrotron sources, allowing small chemical shifts corresponding to chemically distinct species to be more easily seen. For valence levels, higher resolution is also an obvious advantage since, as described earlier, one is usually looking at several lines or bands, which may overlap significantly. Two additional practical points about resolution also should be noted. The spectral resolution of the gratings used to monochromatize synchrotron radiation gets worse as the photon energy gets higher, so the resolution advantage of synchrotron radiation decreases as one goes to high BE core levels. Second, monochromators can be used with laboratory X-ray sources, improving XPS resolution significantly, but not to the degree achievable in UPS or synchrotron work.

The third significant difference between UPS and XPS, from an analytical capability point of view, concerns signal strength. To zeroth order, σ values are a maximum for photon energies just above photoionization threshold, and then decrease strongly as the photon energy is increased, so valence levels in particular have much greater σ values using UPS or synchrotron sources, compared to XPS. When coupled with the high photon fluxes available from such sources, this results in greater absolute sensitivity for UPS or synchrotron spectra.

Taking these differences together, one can see that all three work in favor of UPS or synchrotron compared to XPS when trying to observe very thin layers of chemically distinct material at the surface of a bulk material: improved surface sensitivity; improved resolution allowing small surface chemically shifted components in a spectrum to be distinguished from the underlying bulk signal; and improved absolute sensitivity. As a practical matter, one has to ask whether the core levels one wants to use are even accessible to UPS or synchrotron and whether the need to go to a national facility on a very access-limited basis can compare to day-in, day-out laboratory operations. For UPS using He I and He II radiation sources the addition of these to existing XPS system is not excessively costly and is then always there to provide additional capability useful for specific materials and problems.

The final difference between UPS or synchrotron capabilities and XPS, from an analytical point of view, is in lateral resolution. Modern laboratory XPS small-spot instruments can look at areas down to 30–150 μm, depending on the particular instrument, with one very specialized instrument offering imaging capabilities at 10-μm resolution, but with degraded spectroscopy capabilities.[8] For UPS and synchrotron radiation, much higher spatial resolution can be achieved, partly because the lower kinetic energy of the photoelectron lends itself better to imaging schemes and partly because of efforts to focus synchrotron radiation to small spot sizes. The

potential for a true photoelectron microscope with sub 1000-Å resolution therefore exists, but it has not been realized in any practical sense yet.

Conclusions

UPS, if defined as the use of He I, He II, or other laboratory low-energy radiation sources (<50 eV), has rather limited materials surface analysis capabilities. Valence and core electron energy levels below the energy of the radiation source used can be accessed and the main materials analysis role is in providing higher resolution and high surface sensitivity data as a supplement to XPS data, usually for the purpose of learning more about the chemical bonding state at a surface. Angle-resolved UPS can supply molecular orientation geometric information for ordered structures on single crystal surfaces, but its main use is to provide detailed band structure information.

Synchrotron radiation can be used to provide the same information, but also has the great advantage of a wider, tunable, photon energy range. This allows one to access some core levels at higher resolution and surface sensitivity than can be done by XPS. The variable energy source also allows one to vary the surface sensitivity by varying the kinetic energy of the ejected photoelectrons, thereby creating a depth profiling capability. Most synchrotron photoemission work to date has involved fundamental studies of solid state physics and chemistry, rather than materials analysis, albeit on such technologically important materials as Si, GaAs, and CdTeHg. Some quite applied work has been done related to the processing of these materials, such as studying the effects of cleaning procedures on residual surface contaminants, and studying reactive ion-etching mechanisms.[9] The major drawback of synchrotron radiation is that it is largely unavailable to the analytical community and is an unreliable photon source for those who do have access. As the number of synchrotron facilities increase and as they become more the domain of people wanting to use them as dedicated light sources, rather than in high-energy physics collision experiments, the situation for materials analysis will improve and the advantages over laboratory-based XPS will be more exploitable. Synchrotron radiation will never replace laboratory-based XPS, however, and it should be regarded as complementary, with advantages to be exploited when really needed. High spatial resolution photoelectron microscopy is likely to become one such area.

Related Articles in the Encyclopedia

XPS and SEXAFS

References

1 D. W. Turner, C. Baker, A. D. Baker, and C. R. Brundle. *Molecular Photoelectron Spectroscopy.* Wiley, London, 1970. This volume presents a brief

introduction to the principles of UPS and a large collection of spectra on small molecules, together with their interpretation in terms of the electronic structure and bonding of the molecules.

2 W. E. Spicer. In *Survey of Phenomena in Ionized Gases.* International Atomic Energy Agency, Vienna, 1968, p. 271. A review of the early photoemission work on solids by the pioneering group in this area.

3 D. Menzel. *J. Vac. Sci. Tech.* **12,** 313, 1975. A review of the applications of UPS to the adsorption of molecules at metal surfaces.

4 C. R. Brundle. In *Molecular Spectroscopy.*(A. R. West, Ed.) Heyden, London, 1976. This review discusses both the use of XPS and UPS in studying adsorption and reactions at surfaces.

5 K. Kimura, S. Katsumata, Y. Achita, Y. Yamazaki, and S. Iwata. *Handbook of He I Photoelectron Spectra of Fundamental Organic Molecules.* Halsted Press, New York, 1981. This volume collects together spectra and interpretation for 200 organic molecules.

6 *Photoemission in Solids.* (L. Ley and M. Cardona, Eds.) Springer-Verlag, New York, 1978 and 1979, Vols. 1 and 2.

7 N. V. Smith and F. J. Himpsel. In *Handbook on Synchrotron Radiation.* (E. E. Koch, Ed.) North Holland, New York, 1983, Vol. 1b.

8 P. Coxon, J. Krizek, M. Humpherson, and I. R. M. Wardell. *J. Elec. Spec.* 821, 1990.

9 J. A. Yarmoff and F. R. McFeely, *Surface Science* **184,** 389, 1987.

5.3 AES

Auger Electron Spectroscopy

Y.E. STRAUSSER

Contents

Introduction

Auger electron spectroscopy (AES) is a technique used to identify the elemental composition, and in many cases, the chemical bonding of the atoms in the surface region of solid samples. It can be combined with ion-beam sputtering to remove material from the surface and to continue to monitor the composition and chemistry of the remaining surface as this surface moves into the sample. It uses an electron beam as a probe of the sample surface and its output is the energy distribution of the secondary electrons released by the probe beam from the sample, although only the Auger electron component of the secondaries is used in the analysis.

Auger electron spectroscopy is the most frequently used surface, thin-film, or interface compositional analysis technique. This is because of its very versatile combination of attributes. It has surface specificity—a sampling depth that varies

between 5 and 100 Å depending upon the energy of the Auger electrons measured and the signal-to-noise ratio in the spectrum. It has good lateral spatial resolution, which can be as low as 300 Å, depending on the electron gun used and the sample material. It has very good depth resolution, as low as 20 Å depending on the characteristics of the ion beam used for sputtering. It has a good absolute detectability, as low as 100 ppm for most elements under good conditions. It can produce a three-dimensional map of the composition and chemistry of a volume of a sample that is tens of μm thick and hundreds of μm on a side.

On the other hand, AES cannot detect H or He. It does not do nondestructive depth profiling. It uses an electron beam as a probe, which can be destructive to some samples. It requires the sample to be put into and to be compatible with high vacuum. Some nonconducting samples charge under electron beam probing and cannot be analyzed. The sputtering process can alter the surface composition and thereby give misleading results. It does turn out to be the technique of choice, in its area, much of the time. The purpose of this article is to make clear what it can and cannot do and how to get the most information from it.

The Auger process, which produces an energetic electron in a radiationless atomic transition, was first described by Pierre Auger in 1923.[1] The detection of Auger electrons in the secondary electron energy spectra produced by electron bombardment of solid samples was reported by J. J. Lander in 1953.[2] Its use in an analytical technique to characterize solid surfaces was made practical by Larry Harris' analog detection circuitry in 1967.[3] From that time the technology developed very rapidly, and the technique gained momentum through the 1970s and 1980s.

As the technique developed so did the instrumentation. The hardware development has taken advantage of improvements in ultrahigh vacuum technology and computerization. Systems are available having 300-Å diameter field emission electron beams; user-friendly, rapidly attained ultrahigh vacuum; and complete computer control of the system. At the other end of the price range are components that can be "plugged in" to various deposition and processing systems to provide *in-situ* surface characterization.

AES, X-Ray Photoelectron Spectroscopy (XPS), Secondary Ion Mass Spectroscopy (SIMS), and Rutherford Backscattering Spectroscopy (RBS) have become the standard set of surface, thin-film, and interface analysis tools. Each has its own strengths, and mostly they are complementary. XPS uses X rays as a probe, which are usually less damaging to the surface than the electron beam of Auger but which can't be focused to give high lateral spatial resolution. XPS is also more often selected to determine chemical information. SIMS can detect H and He and has a much higher absolute sensitivity in many cases, but seldom gives any chemical information and, by its nature, has to remove material to do its analysis. RBS readily produces good quantitative results and does nondestructive depth profiling, but it lacks the absolute sensitivity of Auger to many of the important elements and its depth resolution is not as good as Auger can produce, in many cases.

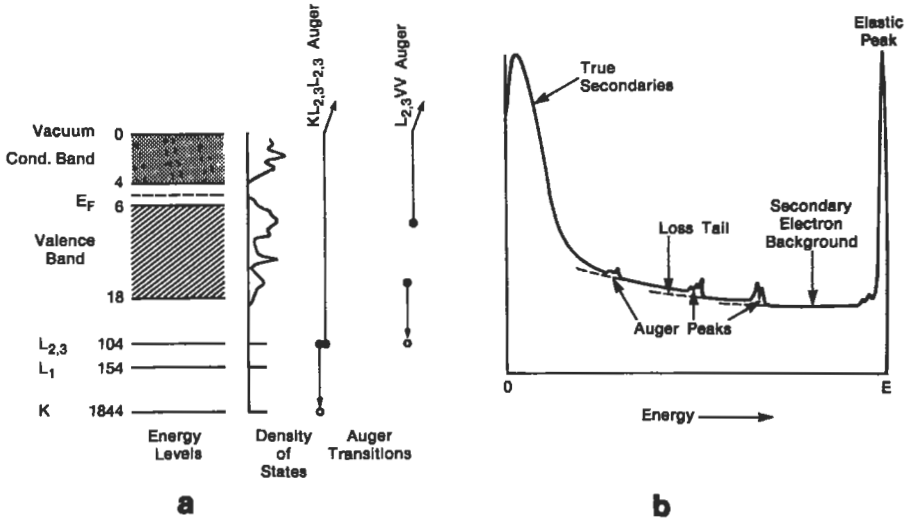

Figure 1 **(a) Energy level diagram of solid Si, including the density of states of the valence and conduction bands, a schematic representation of the Si $KL_{2,3}L_{2,3}$ Auger transitions, and a subsequent LVV Auger transition. (b) The complete secondary electron energy distribution produced by the interaction of a primary electron beam of energy *E* with a solid surface. The true secondary peak, the elastic peak, and some Auger peaks are shown. Also shown are the secondary background and the loss tail contributions to the background from each of the Auger peaks.**

Basic Principles of Auger

The basic Auger process involves the production of an atomic inner shell vacancy, usually by electron bombardment, and the decay of the atom from this excited state by an electronic rearrangement and emission of an energetic electron rather than by emission of electromagnetic radiation. For example, as illustrated in Figure 1a, if a Si surface is bombarded by 5-keV electrons, some of the Si atoms will lose electrons from their K shell, whose binding energy is ~1.8 keV. The K shell vacancy will typically be filled by the decay of an electron from one of the L subshells, let's say the $L_{2,3}$ shell, which has a binding energy of 104 eV. This leaves an energy excess of 1.7 keV. This is sometimes relieved by the emission of a 1.7-keV X ray, which is the basis for the EDS and WDS techniques used in the SEM. Most of the time, however, it is relieved by the ejection of another $L_{2,3}$ shell electron that overcomes its 0.1-keV binding energy and carries off the remaining 1.6 keV of energy. This characteristic energy is the basis for the identification of this electron as having come from a Si atom in the sample. This electron is called a Si $KL_{2,3}L_{2,3}$ Auger electron and the process is called a KLL Auger transition. This process leaves the atom with 2 vacancies in the $L_{2,3}$ shell that may further decay by Auger processes involving

electrons from the Si M shell, which is also the valence band, and thus these Auger transitions are called LVV transitions. The two valence-band electrons involved in an LVV transition may come from any two energy states in the band, although they will most probably come from near peaks in the valence-band density of states, and thus the shape of the LVV "peak" is derived from a self convolution of the valence-band density of states, and the width of the LVV peak is twice the width of the valence band.

The complete description of the number of Auger electrons that are detected in the energy distribution of electrons coming from a surface under bombardment by a primary electron beam contains many factors. They can be separated into contributions from four basic processes, the creation of inner shell vacancies in atoms of the sample, the emission of electrons as a result of Auger processes resulting from these inner shell vacancies, the transport of those electrons out of the sample, and the detection and measurement of the energy distribution of the electrons coming from the sample.

In fact, Auger electrons are generated in transitions back to the ground state of atoms with inner shell vacancies, no matter what process produced the inner shell vacancy. Auger peaks are therefore observed in electron energy spectra generated by electron excitation, X-ray excitation, and ion excitation, as well as in certain nuclear reactions. The technique usually referred to as Auger electron spectroscopy uses excitation by an electron beam. The spectra produced by X-ray excitation in XPS routinely also include Auger peaks mixed in with the photoelectron peaks. Ion beam-induced Auger peaks occur, at times, during the depth profiling mode of analysis in AES.

Production of Inner Shell Vacancies

The probability (cross section) that a high-energy incident electron will produce a particular inner shell vacancy in a certain element is a function of the ratio of the primary electron energy to the binding energy of the electrons in that shell. In general the cross section rises steeply from 0 at a ratio of 1 to a maximum at a ratio in the range from 3 to 6 and then decreases gradually as the ratio increases further. As an example, the Si K shell binding energy is 1844 eV. To get the maximum yield of Si K shell vacancies, and therefore Si KLL Auger electrons, a primary electron-beam energy of 5.5–11.0 keV should be used. On the other hand if better surface sensitivity is needed (see below) the low-energy Si LVV transition is preferred. The Si L shell binding energies are 154 and 104 eV, so the primary beam energy would be optimized at 0.3–0.9 keV for these transitions.

Auger Electron Emission

Once an inner shell vacancy is created in an atom the atom may then return toward its ground state via emission of a characteristic X ray or through a radiationless Auger transition. The probability of X-ray emission is called the fluorescence yield.

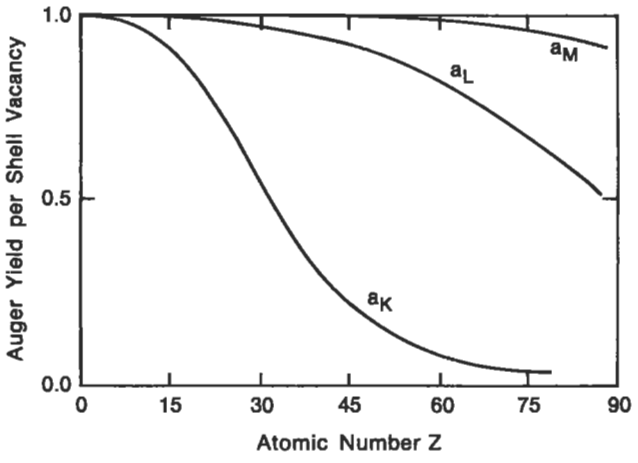

Figure 2 **Percentage of inner shell vacancies resulting in Auger electron emission for holes in the K, L, and M shells.**

The Auger yield is 1 minus the fluorescence yield, since these are the only two options. Figure 2 shows the Auger yield as a function of atomic number for initial vacancies in the K, L, and M shells. It is clear that Auger emission is the preferred decay mechanism for K shell vacancies in the low atomic number elements, and for L and M shell initial vacancies for all elements. By properly selecting the Auger transition to monitor, all elements (except H and He) can be detected using Auger transitions that have a 90% or higher Auger yield per initial vacancy.

Electron Transport to the Surface

As the various electrons, including Auger electrons, resulting from primary electron bombardment diffuse through the sample and to the surface many scattering events occur. The inelastic collisions have the effect of smoothing the energy distribution of these electrons and result in a power law energy distribution[4] at energies between the elastic peak and the "true secondary" peak, which occur at the high-energy and low-energy end of the distribution, respectively. This produces a background, as shown in Figure 1b, on which the Auger peaks are superimposed, that can be modeled and removed (see below). Inelastic collisions also have the effect of removing some of the Auger electrons from their characteristic energy position in an Auger peak and transferring them to lower energies as part of the "loss tail," which starts at the low-energy side of the Auger peak and extends all the way to zero energy.

The inelastic collision process is characterized by an inelastic mean free path, which is the distance traveled after which only $1/e$ of the Auger electrons maintain their initial energy. This is very important because only the electrons that escape the sample with their characteristic Auger energy are useful in identifying the atoms in

the sample. This process gives the technique its surface specificity. This inelastic mean free path is a function, primarily, of the energy of the electron and, secondarily, of the material through which the electron is traveling. Figure 6 in the XPS article shows many measurements of the inelastic mean free path in various materials and over a wide range of energies, and an estimate of a universal (valid for all materials) inelastic mean free path curve versus energy.

The minimum in the mean free path curve, at around 80 eV, is the energy at which electrons travel the shortest distance before suffering an energy-altering scattering event. Thus Auger electrons that happen to have their energy in this vicinity will be those that will have the thinnest sampling depth at the surface. For example, while Si LVV Auger electrons from oxidized Si (at approximately 78-eV) are generated at depths ranging from the top monolayer to nearly a μm from a primary electron beam with a typical 5-keV energy, 63% of the electrons that escape without losing any energy come from the top 5 Å of the sample. Furthermore, 87% are contributed by the top 10 Å of the sample and 95% have been produced in the top 15 Å of material. The depth from which there is no longer any signal contribution is ultimately determined by the signal-to-noise ratio in the measured spectrum. If a 5% signal variation is accurately measurable then atoms 3 mean free paths down contribute to the measurement. If 2% of the signal is well above the noise level then atoms at a depth of 4 mean free paths contribute to the measurement.

Secondary Electron Collection

As the electrons leave the surface they move in a cosine-shaped intensity distribution away from the analysis point and travel in straight lines until they enter the energy analyzer. The entrance slit of the energy analyzer determines the percentage that are collected, but it is typically just under 20% for the most commonly used energy analyzer, the cylindrical mirror analyzer (CMA). Once in the energy analyzer more electrons are lost by scattering at grids and the CMA transmission is typically 60%.

Information in Auger Spectra

Using the best procedures during data acquisition produces spectra with the maximum available information content. Once spectra are recorded that contain the information that is sought using the best procedures for extracting the information from the data is important to maximize the value of the analysis. This section will consider the procedures for data acquisition and the extraction of various types of information available from the data.

Data Acquisition

For primarily historical reasons people have come to consider Auger spectra as having the form, $dN(E)/dE$ versus E, where $N(E)$ is the energy distribution of the sec-

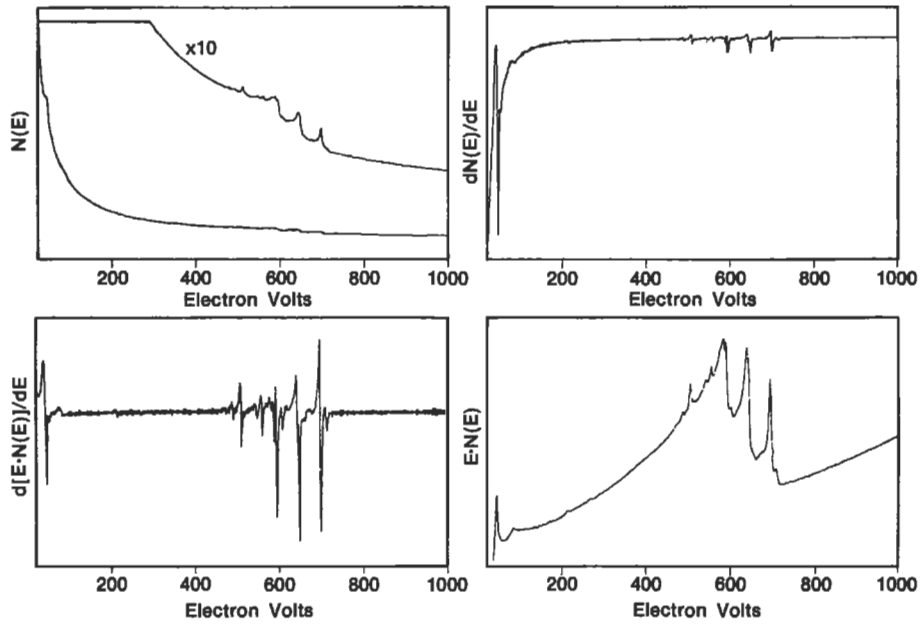

Figure 3 **The $N(E)$, $dN(E)/dE$, $dEN(E/dE$, and $EN(E)$ forms of secondary electron energy spectra from a slightly contaminated Fe surface.**

ondary electrons being detected and E is their energy. This came about because of the properties of various energy analyzers used and because of peculiarities of the analog electronics used to run them. Spectra in this form were acquired by adding an AC component to the energy-selecting voltage of the energy analyzers (a modulation) and detecting the signal with a lock-in amplifier.[5] This led to the signal being acquired in the differential mode, $dN(E)/dE$ versus E, instead of $N(E)$ versus E. These forms of acquired spectra are shown in Figure 3. With the advent of the CMA and computer-controlled digital signal acquisition, which can be coupled with either pulse counting or voltage-to-frequency conversion for decoupling the signal from the high positive collection voltage, it has finally become practical to discard the modulation and the lock-in amplifier in signal acquisition, as is done in Figure 3(bottom right panel). Acquiring data directly in $N(E)$ (or $E\times N(E)$) form, followed by subsequent mathematical processing, provides six valuable advantages:

1 There is an improved signal-to-noise ratio in the raw data. This can be seen in the $E\times N(E)$ form of data in Figure 3.

2 The energy analyzer is always operated at its best energy resolution.

3 The measured Auger signal is proportional to the number of atoms sampled. In the derivative mode of data acquisition this is frequently not the case, for example, if an inappropriate modulation voltage is used or if the line shape has

changed due to a change in chemical environment.

4 The physical information in the line shape is immediately available for observation.

5 Peak overlaps can be eliminated simply by peak fitting and subtraction.

6 Loss tail analysis can be applied to the data. (This procedure is discussed below.)

Thus it is best to acquire and store the data in the simplest and least-processed form possible.

Extracting Information From the Data

There are at least four kinds of information available from an Auger spectrum. The simplest and by far most frequently used is qualitative information, indicating which elements are present within the sampling volume of the measurement. Next there is quantitative information, which requires a little more care during acquisition to make it extractable, and a little more effort to extract it, but which tells how much of each of the elements is present. Third, there is chemical information which shows the chemical state in which these elements are present. Last, but by far the least used, there is information on the electronic structure of the material, such as the valance-band density of states that is folded into the line shape of transitions involving valance-band electrons. There are considerations to keep in mind in extracting each of these kinds of information.

Qualitative Information

Qualitative information can be extracted from Auger spectra quite simply, by a trained eye or by reference to one of the available Auger charts, tables of energies, or handbooks of spectra. The most basic identification is done from the energies of the major peaks in the spectrum. The next level of filtration is done from the peak intensity ratios in the patterns of peaks in the spectra of the elements present. One of the charts of Auger peak energies available is shown in Figure 4. The useful Auger spectra of the elements fall into groups according to the transition type, KLL, LMM, MNN, etc. If you look across the chart, following a given energy, it is clear that there are many possibilities for intermixing of patterns from different elements, but there are few direct peak overlaps. Generally, if there are peaks from two elements that interfere, there are other peaks from both those elements that do not overlap. One of the most difficult exceptions to this rule is in the case of B and Cl: B has only one peak, a KLL peak at 180 eV. Cl has an LMM peak at 180 eV and its KLL peaks are at 2200–2400 eV, high enough that they are seldom recorded. If there is a real uncertainty as to which of these elements is present, it is necessary to look for the latter peaks.

Peak overlaps that totally obscure one of the elements in the spectrum have been shown to be separable.[6] A Co–Ni alloy film under a Cu film is a combination that produces a spectrum where the Ni peaks are all overlapped by Cu or Co peaks, or

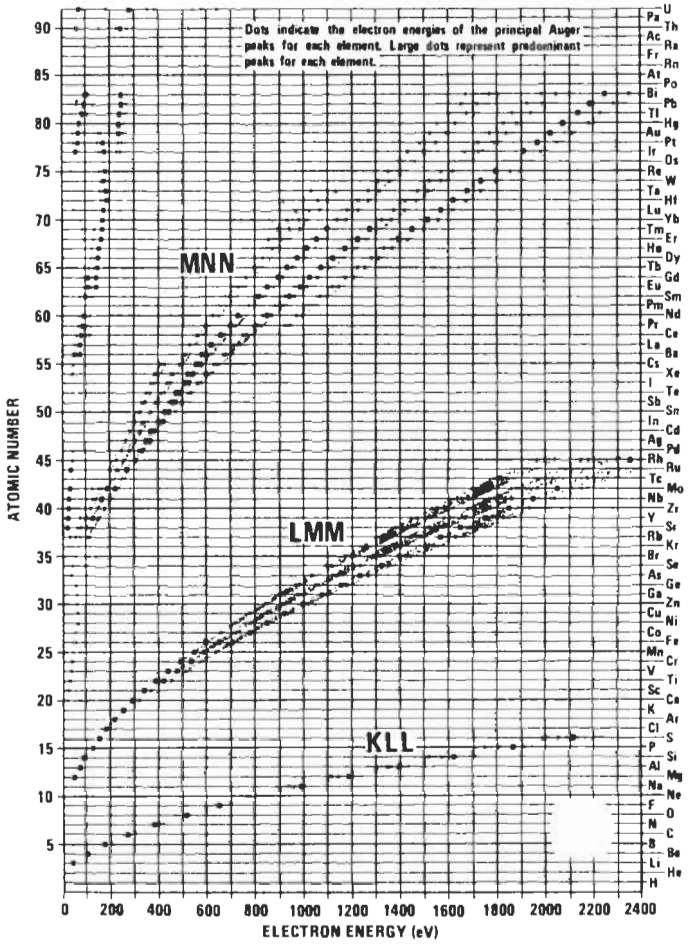

Figure 4 **One of the numerous available charts of Auger electron energies of the elements.**

both. The intensities in the Cu and Co patterns show that another element is present. With the use of background subtraction, standard spectra, and peak fitting and subtraction, the Ni spectrum was uncovered and identified, and even quantitative information, with identified accuracy limitations, was obtained.

When listing the elements present from qualitative analysis, the issues of sensitivity and signal-to-noise level arise. The minimum amount of an element that must be present to be detected in an Auger spectrum is a function of a number of variables. Some of these are determined by the element, such as its ionization cross section at the primary energy being used, the Auger yield from its most prolific inner shell vacancy, the energy of its Auger electron (since this determines the elec-

trons' mean free path for escape from the solid), etc. Other variables are under the control of the measurement parameters, such as the primary beam energy and current, the energy resolution of the energy analyzer, the angle of incidence of the primary beam onto the sample and the acceptance angle of the energy analyzer. These variables can, to a certain degree, be controlled to yield the maximum signal-to-noise ratio for the element of interest. When these parameters are optimized the detection limit for most elements is on the order of a few times $10^{18}/cm^3$ homogeneously distributed, or about 1 atom in 10,000.

Quantitative Information

The number of Auger electrons from a particular element emitted from a volume of material under electron bombardment is proportional to the number of atoms of that element in the volume. However it is seldom possible to make a basic, first principles calculation of the concentration of a particular species from an Auger spectrum. Instead, sensitivity factors are used to account for the unknown parameters in the measurement and applied to the signals of all of the species present which are then summed and each divided by the total to calculate the relative atomic percentages present.

Of the total number of Auger electrons emitted only a fraction escapes the sample without energy loss. The rest become part of the loss tail on the low-energy side of the Auger peak extending to zero energy and contribute to the background under all of the lower energy Auger peaks in the spectrum. This process must be taken into account when using a sensitivity factor for a particular Auger system. Sensitivity factors are usually taken from pure elemental samples or pure compound samples. This means that the element is homogeneously distributed in the standard. If this is not true in the unknown sample, the percentage of Auger electrons that escape the sample without energy loss changes. If the element is concentrated at the surface, fewer Auger electrons will suffer energy loss; if it is concentrated in a layer beneath another film, more Auger electrons will suffer energy loss before they escape the sample. This can be seen in Figure 5, which shows oxygen in a homogeneous SiO_2 film, in a surface oxide on Si, and from an SiO_2 film under a layer of Si. An oxygen sensitivity factor determined from a homogeneous sample would not properly represent the oxygen concentration in the lower two spectra of Figure 5.

Sensitivity factors should be measured on the same energy analyzer, at the same energy resolution, at the same primary electron beam energy, and at the same sample orientation to the electron beam and energy analyzer, as the spectra to which they are applied. Only when these precautions are taken can any sort of quantitative accuracy be expected. Even with these precautions the oxygen example discussed above and shown in Figure 5 would present a problem. The most direct way to prevent this problem is by the process referred to above as "loss tail analysis." This involves comparing the ratios of the peak heights to the loss tail heights, on background subtracted spectra, from the spectrum of the unknown sample and the

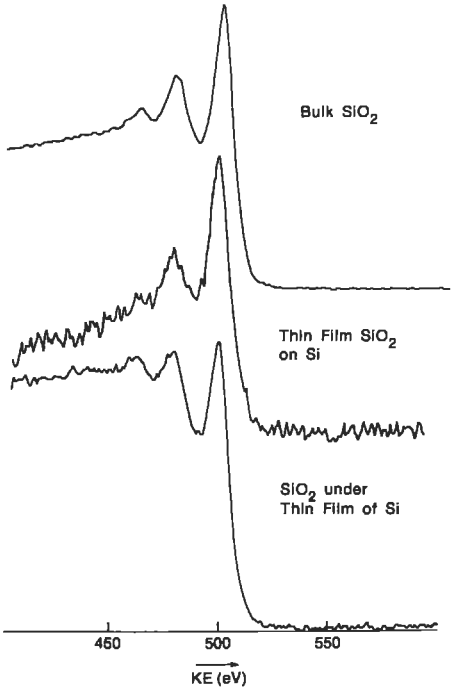

Figure 5 **Oxygen spectra from bulk SiO_2, a thin film of SiO_2 on Si, and SiO_2 under a thin film of Si. These spectra have had their background removed, and so the loss tail can be seen as the height of the spectra at energies below the peaks.**

spectrum from which the sensitivity factor was determined. When these ratios are equal the same degree of depth homogeneity of the element in question is assured.

Chemical Information

There is a great deal of chemical information in the line shapes and chemical shifts of peaks in Auger spectra. XPS is generally considered to be a more appropriate tool to determine chemistry in a sample. It is true that the photoelectron lines used in XPS are typically narrower and that therefore smaller chemically induced energy shifts can be detected. Moreover, the energy analyzers used in XPS often have better energy resolution. However, it is also true that the chemically induced energy shifts in Auger peaks are usually larger than the corresponding shifts in photoelectron peaks.[7]

Chemical information is present in Auger spectra in two forms; a shift in the energy of the peak maximum and sometimes as a change in the line shape of the Auger peak. Line shape changes are greatest in transitions involving valance-band electrons, such as the LVV transition in Si. Since this line shape is just a weighted

9.1 RBS

Rutherford Backscattering Spectrometry

SCOTT M. BAUMANN

Contents

Introduction

Rutherford Backscattering Spectrometry (RBS) is one of the more quantitative depth-profiling techniques available, with typical accuracies of a few percent. The depth profiling is done in a nondestructive manner, i.e., not by sputtering away the surface layers. Results obtained by RBS are insensitive to sample matrix and typically do not require the use of standards, which makes RBS the analysis of choice for depth profiling of major constituents in thin films. Detection limits range from a few parts per million (ppm) for heavy elements to a few percent for light elements. RBS depth resolution is on the order of 20–30 nm, but can be as low as 2–3 nm near the surface of a sample. Typical analysis depths are less than 2000 nm, but the use of protons, rather than helium, as the probe particle can increase the sampling depth by as much as an order of magnitude. Lateral resolution for most instruments is on the order of 1–2 millimeters, but some microbeam systems have a resolution on the order of 1–10 μm.

Three common uses of RBS analysis exist: quantitative depth profiling, areal concentration measurements (atoms/cm^2), and crystal quality and impurity lattice site analysis. Its primary application is quantitative depth profiling of semiconductor thin films and multilayered structures. It is also used to measure contaminants and to study crystal structures, also primarily in semiconductor materials. Other applications include depth profiling of polymers,[1] high-T_C superconductors, optical coatings, and catalyst particles.[2]

Recent advances in accelerator technology have reduced the cost and size of an RBS instrument to equal to or less than many other analytical instruments, and the development of dedicated RBS systems has resulted in increasing application of the technique, especially in industry, to areas of materials science, chemistry, geology, and biology, and also in the realm of particle physics. However, due to its historical segregation into physics rather than analytical chemistry, RBS still is not as readily available as some other techniques and is often overlooked as an analytical tool.

Basic Principles

RBS is based on collisions between atomic nuclei and derives its name from Lord Ernest Rutherford who first presented the concept of atoms having nuclei. When a sample is bombarded with a beam of high-energy particles, the vast majority of particles are implanted into the material and do not escape. This is because the diameter of an atomic nucleus is on the order of 10^{-4} Å while the spacing between nuclei is on the order of 1 Å. A small fraction of the incident particles do undergo a direct collision with a nucleus of one of the atoms in the upper few μm of the sample. This "collision" actually is due to the Coulombic force present between two nuclei in close proximity to each other, but can be modeled as an elastic collision using classical physics.

The energy of a backscattered particle detected at a given angle depends upon two processes: the loss of energy by the particle due to the transfer of momentum to the target atom during the backscattering event, and the loss of energy by the particle during transmission through the sample material (both before and after scattering). Figure 1 is a schematic showing backscattering events occurring at the surface of a sample and at a given depth d in the sample. For scattering at the sample's surface the only energy loss is due to momentum transfer to the target atom. The ratio of the projectile's energy after a collision to the its energy before a collision (E_1/E_0) is defined as the kinematic factor K:[3,4]

$$K = \left(\frac{\sqrt{1 - ((M_1/M_2)\sin\theta)^2} + (M_1/M_2)\cos\theta}{1 + (M_1/M_2)} \right)^2 \tag{1}$$

where M_1 is the mass of the incident particle (typically ^{4}He); M_2 is the mass of the target atom; and R is defined as the angle between the trajectory of the He particle before and after scattering.

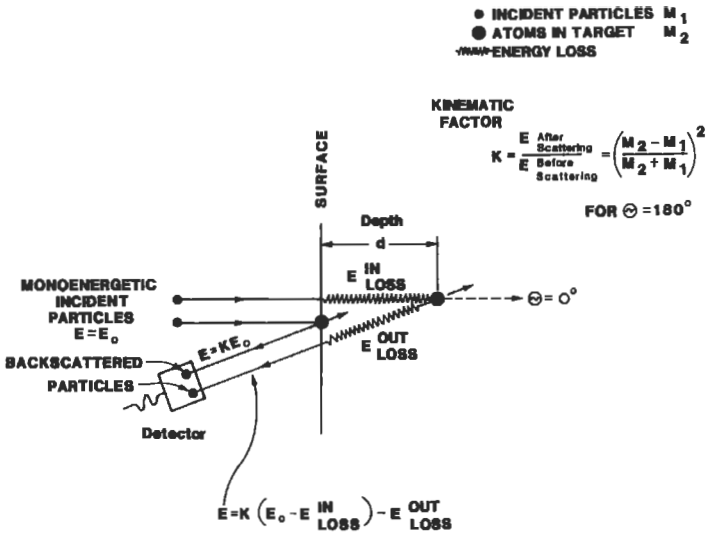

Figure 1 **A schematic showing the various energy loss processes for backscattering from a given depth in a sample. Energy is lost by momentum transfer between the probe particle and the target particle, and as the probing particle traverses the sample material both before and after scattering.**

As shown in Figure 1, when the probing particles penetrate to some depth in a sample, energy is lost in glancing collisions with the nuclei of the target atoms as well as in interactions with electrons. For a 2-MeV He atom, the energy loss is in the range of 100–800 eV/nm and depends upon the composition and density of the sample. This means that a particle that backscatters from some depth in a sample will have measurably less energy than a particle that backscatters from the same element on the sample's surface. This allows one to use RBS in determining the thickness of layers and in depth profiling.

The relative number of particles backscattered from a target atom into a given solid angle for a given number of incident particles is related to the differential scattering cross section:

$$\frac{d\sigma}{d\Omega} = \left(\frac{Z_1 Z_2 e^2}{4E}\right)^2 \frac{4\left(\sqrt{1 - \left((M_1/M_2)\sin\theta\right)^2} + \cos\theta\right)^2}{(\sin\theta)^4 \sqrt{1 - \left((M_1/M_2)\sin\theta\right)^2}} \tag{2}$$

where Z_1 and Z_2 are the atomic numbers of the incident atom and the target atom, E is the energy of the incident atom immediately before scattering, and e is the electronic charge. A rule of thumb is that the scattering cross section is basically proportional to the square of the atomic number Z of the target species. This means that RBS is more than a hundred times more sensitive for heavy elements than for light

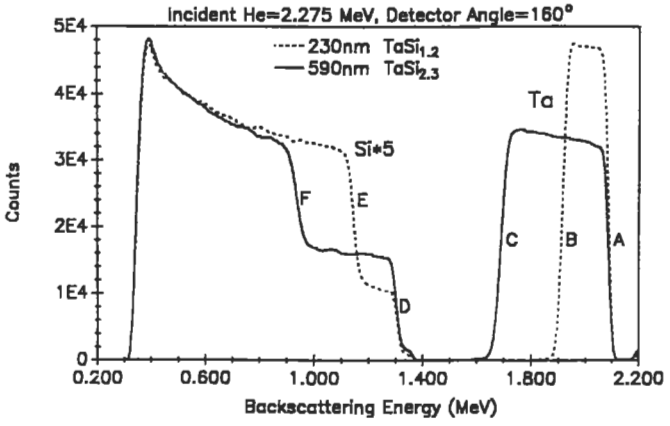

Figure 2 **RBS spectra from two $TaSi_x$ films with different Si / Ta ratios and layer thicknesses.**

elements, such as B or C. There is much greater separation between the energies of particles backscattered from light elements than from heavy elements, because a significant amount of momentum is transferred from an incident particle to a light target atom. As the mass of the target atom increases, less momentum is transferred to them and the energy of the backscattered particle asymptotically approaches the incident particle energy (see Equation 1). This means that RBS has good mass resolution for light elements, but poor mass resolution for heavy elements. For example, it is possible to resolve C from O or P from Si but it is not possible to resolve W from Ta, or Fe from Ni when these elements are present at the same depths in the sample, even though the difference in mass between the elements in each of these pairs is roughly 1 amu.

Figure 2 shows how the processes combine to create an RBS spectrum by displaying the spectra from two $TaSi_x$ films on Si substrates. Metal silicide films are commonly used as interconnects between semiconductor devices because they have lower resistivity than aluminum or polysilicon. The resistivity of the film depends upon the ratio of Si to metal and on the film thickness, both of which can be determined by RBS. The peak in each spectrum at high energy is due to scattering from Ta in the $TaSi_x$ layers while the peak at lower energy is from Si in the $TaSi_x$ layer and the Si substrate. The high-energy edge of the Ta peaks near 2.1 MeV (labeled *A*) corresponds to scattering from Ta at the surface of both samples, while the high-energy edge of the Si peaks (labeled *D*) near 1.3 MeV corresponds to backscattering from Si at the surface of the $TaSi_x$ layer. By measuring the energy width of the Ta peak or the Si step and dividing by the energy loss of He (the incident particle) per unit depth in a $TaSi_x$ matrix, the thickness of the $TaSi_x$ layer can be calculated. For example, the low-energy edge of the Ta peak corresponds to scattering from Ta at the $TaSi_x$–Si interface and the step in the Si peak corresponds to the increase in the

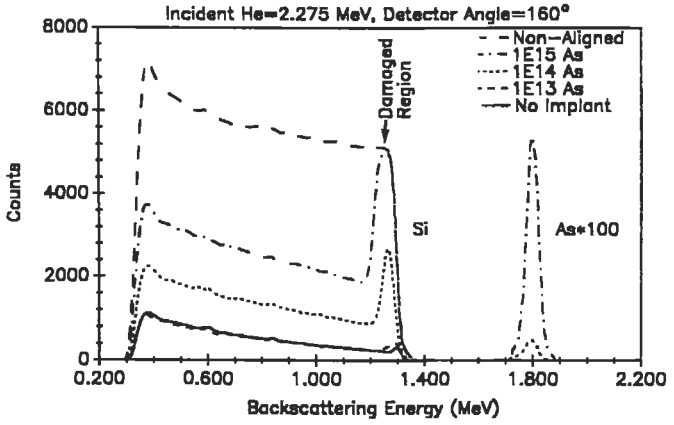

Figure 3 **Crystal channeled RBS spectra from Si samples implanted with 10^{13}, 10^{14}, and 10^{15} As atoms/cm^2. Also shown is a channeled spectrum from a nonimplanted Si sample and a nonaligned, or random, Si spectrum.**

Si concentration at the $TaSi_x$–Si interface. In this example, one of the films is 230 nm thick, while the other film is 590 nm thick. Particles scattered from Ta at the $TaSi_x$–Si interface of the 230-nm film have a final energy of about 1.9 MeV (labeled *B*) after escaping from the sample, while particles scattered from Ta at the $TaSi_x$–Si interface of the 590-nm film have a final energy of about 1.7 MeV (labeled *C*). Similarly, particles scattered from Si at the $TaSi_x$–Si interface of the 230-nm film have a final energy of about 1.1 MeV (labeled *E*) after escaping from the sample, while particles scattered from Si at the $TaSi_x$–Si interface of the 590-nm film have a final energy of about 0.9 MeV (labeled *F*). In these spectra the greater energy width of the Ta peak and the Si step for the 590-nm $TaSi_x$ film are directly related to the greater thickness of the film.

By measuring the height of the Ta and Si peaks and normalizing by the scattering cross section for the respective element, the ratio of Si to Ta can be obtained at any given depth in the film. Due to the smaller scattering cross section for Si, the Si peaks in Figure 3 have been multiplied by a factor of 5. The height of a backscattering peak for a given layer is inversely proportional to the stopping cross section for that layer, and in this case the stopping cross section of $TaSi_{2.3}$ is 1.37 times greater than that of Si. This explains why, even for the film with a Si/Ta ratio of 2.3, the height of the peak corresponding to Si in the $TaSi_x$ layer is less than ½ the height of the peak corresponding to Si in the sample substrate.

Channeling

In addition to elemental compositional information, RBS also can be used to study the structure of single-crystal samples.[5, 6] When a sample is *channeled*, the rows of atoms in the lattice are aligned parallel to the incident He ion beam. The bombard-

ing He will backscatter from the first few monolayers of material at the same rate as a nonaligned sample, but backscattering from buried atoms in the lattice will be drastically reduced, since these atoms are shielded from the incident particles by the atoms in the surface layers. For example, the backscattering signal from a single-crystal Si sample that is in channeling alignment along the (100) axis will be approximately 3% of the backscattering signal from a nonaligned crystal, or amorphous or polycrystalline Si. By measuring the reduction in backscattering when a sample is channeled it is possible to quantitatively measure and profile the crystal perfection of a sample, or to determine its crystal orientation.

Figure 3 shows channeled spectra from a series of Si samples that were implanted with 10^{13}, 10^{14}, and 10^{15} arsenic atoms/cm^2. Only the As peaks for the two highest dose implants are shown, but with a longer data acquisition time the concentration 10^{13} As atoms/cm^2 could be detected. The damage caused to the Si crystal lattice by the As implants is reflected in the peaks near 1.25 MeV in the aligned spectra. In the case of the 10^{15}-atoms/cm^2 implant there is little or no single-crystal structure remaining in the damaged region of the Si, so the backscattering signal is the same height as for nonaligned Si. Measuring the energy width of the damage peak indicates that the damaged layer is approximately 200 nm thick. Integrating the damage peak and subtracting the backscattering signal obtained for the nonimplanted reference indicates that approximately 1.0×10^{18} Si atoms/cm^2 were displaced by the 10^{15}-atoms/cm^2 As implant, while 3.4×10^{17} and 1.7×10^{16} Si atoms/cm^2 were displaced by the 10^{14}-atoms/cm^2 and 10^{13}-atoms/cm^2 As implants, respectively. In this case RBS could be used to measure accurately the total concentration of arsenic atoms implanted in each sample, to profile the As implant, to determine the amount of As that is substitutional in the Si lattice and its lattice location, to measure the number of displaced Si atoms/cm^2, and to profile the damage in the Si crystal.

Quantification

As noted above, the calculation of elemental concentrations and thicknesses by RBS depends upon the scattering cross section of the element of interest and the stopping cross section of the sample matrix. The scattering and stopping cross sections for each element have been carefully measured and tabulated.[3, 4, 7] In general, scattering cross sections follow the Rutherford scattering model to within 5%. It is difficult to accurately describe the stopping cross sections for all elements with a single equation, so semiempirical values are employed. A polynomial equation with several terms is used so that the stopping cross sections for each element can be calculated over a range of energies. In general, the calculated stopping cross sections are accurate to 10% or better. The stopping cross section for a multi-elemental sample is calculated by normalizing the stopping cross section of each element to its concentration in the sample.

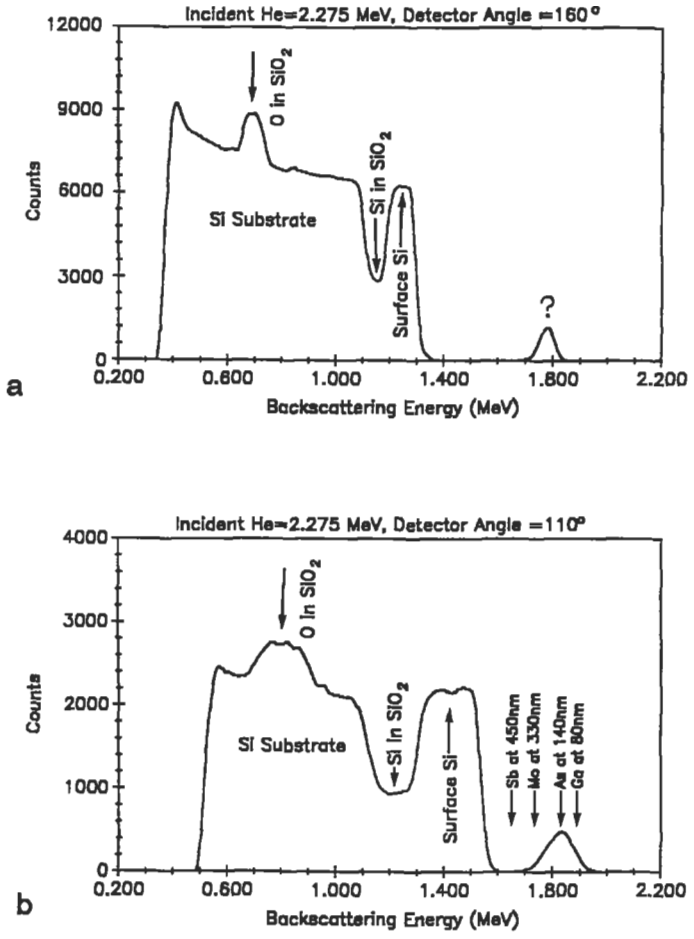

Figure 4 **RBS spectra from a sample consisting of 240 nm of Si on 170 nm of SiO_2 on a Si substrate. The spectrum in (a) was acquired using a scattering angle of 160° while the spectrum in (b) used a detector angle of 110°. This sample was implanted with 2.50×10^{16} As atoms/cm^2, but the As peak cannot be positively identified from either spectrum alone. Only As at a depth of 140 nm will produce the correct peak in both spectra.**

Due to the convoluted mass and depth scales present in an RBS spectrum, it may not be possible to accurately describe an unknown sample using a single RBS spectrum. For example, Figure 4a is an RBS spectrum acquired at a backscattering angle of 160° from a sample implanted with 2.50×10^{16} atoms/cm^2 of As at a depth of approximately 140 nm. If this were a totally unknown sample it would not be possible to determine positively the mass and depth of the implanted species from this spectrum alone, since the peak in the RBS spectrum also could have been caused by a heavier element at greater depth, such as Sb at 450 nm, or Mo at 330 nm, or by a

9.4 ISS

Ion Scattering Spectroscopy

GENE R. SPARROW

Contents

Introduction

Ion Scattering Spectroscopy (ISS) is one of the most powerful and practical methods of surface analysis available. However, it is underutilized due to a lack of understanding about its application and capabilities. This stems from its history, the limited number of high-performance instruments manufactured, and the small number of experienced surface scientists who have actually used ISS in extensive applications. Ironically, it is one of the easiest and most convenient surface analytical instruments to use and it provides useful information for almost any type of solid material.

The most useful application of ISS is in the detection and identification of surface contamination, which is one of the major causes of product failures and problems in product development. The surface composition of a solid material is almost always different than its bulk. Therefore, surface chemistry is usually the study of unknown surfaces of solid materials. To better understand the concept of "surface analysis," which is used very loosely among many scientists, we must first establish a definition for that term. This is particularly important when considering ISS

because of its extreme sensitivity to the surface. In most applications *surface analysis* implies the analysis of a finite thickness or depth of the outermost layers of a material, generally from the outer few atomic layers to a depth of 100–200 Å. Techniques encompassing layers greater than that are better described as thin-film analyses, or as depth profiles directed at obtaining other information. Techniques like Energy-Dispersive X-Ray Spectroscopy (EDS) and FTIR with ATR (Attenuated Total Reflection) generally do not fit the description of surface analysis. Other techniques, such as Auger and ESCA, meet the definition by obtaining spectra that originate from a depth of up to approximately 50–80 Å.

ISS is the most surface sensitive technique known. It is routinely sensitive to the outermost layer of atoms. At this level of depth sensitivity, it can be shown by ISS that most practical solid materials have the same outer atomic layer, i.e., a layer of surface water molecules, or organic material, with the hydrogen oriented upward. Therefore in ISS, as in SIMS using low-energy ions, it is important to include spectra from several different sputtered depths into the surface or to specify the sputtered depth from which the spectrum was obtained. Usually a series of ISS spectra are obtained at successively greater depths into the surface and the resulting spectra are displayed to show the changing composition versus depth. Because of the extreme surface sensitivity of ISS, these depth profiles offer details about changes in surface composition in the outer 50 Å that are generally not obtainable by other techniques. These details are extremely important in many applications, such as the initiation of corrosion, adhesion, bonding, thin-film coatings, lubrication, and electrical contact resistance. Typical data and applications will be discussed.

History

Earlier studies of ion scattering were directed primarily at gas–ion interactions. As studies of ion–solid surfaces became common the energy of the scattered ions was eventually related mathematically to a simple binary elastic event involving a single atom on a surface element and a single probe ion.

The practical use of ion scattering was not developed until the late 1960s when David P. Smith of 3M Company first reported the use of low-energy inert ion scattering to analyze the composition of surfaces. This early pioneering work established ion scattering as a very useful and viable spectroscopy for studying surfaces. The first studies and instruments consisted of simple systems where the ion beam scattered through an angle of 90°; thus accepting only a small solid angle of the signal. Modern systems use ion beams that are coaxial with the detector and exhibit orders of magnitude higher sensitivity. These devices make use of a Cylindrical Mirror Analyzer (CMA) and include detection of ions scattered about a 360° solid angle. A typical device is shown in Figure 1. ISS has since become readily available commercially and is recognized as one of the four major surface techniques, generally including ESCA (XPS), Auger, and SIMS as well.

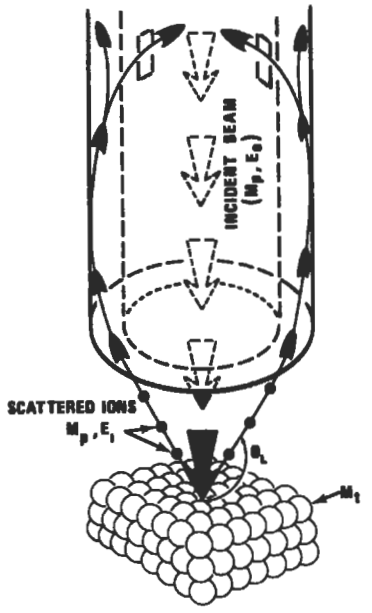

Figure 1 **Schematic of CMA ISS device showing primary ion beam, analyzer, and scattering at 138°.**

Basic Principles

ISS is relatively simple in principle and application. When a low-energy (100–5000 eV) beam of positive ions of some inert element, such as He, Ne, or Ar, strikes a surface, some of the ions are reflected back from the surface. This scattering process involves a single surface atom and a single incident ion. It is, therefore, a simple binary elastic collision that follows all the rules of classical physics. The incident ion scatters back with a loss of energy that depends only on the mass of the surface atom (element) with which the collision occurred. The heavier the surface atom, the smaller the change in energy of the scattered ion. Thus carbon, which is a light atom of mass 12, is readily displaced and the probe ion loses most of its energy, whereas a heavy atom like Pb, having mass 208, is not easily moved. An ion scattering from Pb retains most of its incoming energy. To obtain a spectrum, one merely records the number of scattered ions as their energy is scanned from near 0 eV to the energy of the primary incoming beam. Each element has a unique mass and therefore a unique energy at which the probe ion scatters. The energy of the scattered ion is mathematically related to the mass of the surface atom by the following equation:

$$\frac{E_1}{E_0} = E_r = \frac{M_1^2}{(M_1 + M_2)^2}\left(\cos\theta + \sqrt{\left(\frac{M_2}{M_1}\right)^2 - (\sin\theta)^2}\right)^2$$

where E_0 is the energy of the incident probe ion, E_1 is the energy of the ion scattered from surface atom, E_r is the ratio of the energies of the scattered and probe ions, M_1 is the mass of the primary ion, M_2 is the mass of the surface atom, and θ is the scattering angle measured from the direction of the ion beam.

Penetration of the incident beam below the very outermost atomic layer causes excessive and nondiscrete loss of energy such that the scattered ions do not yield sharp, discrete peaks. Only ions scattered from the outer atomic layer of a surface give rise to a sharp peak. ISS is therefore extremely sensitive to the surface and essentially detects only the outermost surface layer. To obtain more extensive surface information, it is therefore common to continuously monitor the ISS spectrum while sputtering into the surface. When the sputtering is done very slowly using a light atom, such as isotopically pure $^3He^+$, complete spectra can be obtained at successively greater depths into the surface. In routine practice, sputter rates on the order of about 1 to 5 Å per minute are used and approximately 15–20 ISS spectra are obtained throughout a sputtered depth of about 100 Å. Since the most important information is obtained near the surface, the majority of these spectra are obtained in the first few minutes of sputtering.

As the scattering angle θ is decreased to 90°, the physical size of the CMA must increase, until finally one cannot use a CMA but must resort to a sector analyzer. This decreases detection sensitivity by 2–3 orders of magnitude, increases multiple scattering at energies above the primary peaks, and requires much more precise positioning of the sample. Changing the mass of the primary ion beam gas controls not only the sputtering rate of the surface but also changes the spectral resolution and detection sensitivity. For example, using $^3He^+$ permits good detection of C, N, and O, whereas using $^4He^+$ does not. Using Ar^+ provides high sputtering rates for deeper profiles but does not permit the detection of elements having mass less than Ca. Argon also provides increased spectral resolution for higher elements not resolved by He. It is common to sometimes mix Ar and He to detect all elements while obtaining a high sputtering rate. Increasing the energy of the primary beam to above about 3000 eV dramatically increases the overall spectral background, thus decreasing sensitivity, but the spectral resolution increases. Decreasing the beam energy decreases this background and dramatically decreases the sputtering rate. It is possible to obtain useful ISS spectra at energies below 200 eV of He at less than a few nA. The sputtering rate under these conditions is extremely low.

During normal operation, the entire ISS spectrum, covering all elements, is scanned in about 1 second. A number of these scans are then added for signal enhancement and to control the predetermined depth to which sputtering is